Molecular Cell

TSPYL5 depletion induces specific death of ALT cells through USP7-dependent proteasomal degradation of POT1

--Manuscript Draft--

Manuscript Number:	MOLECULAR-CELL-D-18-01834R4
Full Title:	TSPYL5 depletion induces specific death of ALT cells through USP7-dependent proteasomal degradation of POT1
Article Type:	Research Article
Keywords:	Testis Specific Y-encoded-Like Protein 5; Alternative mechanism of telomere lengthening; PML body; POT1; USP7; TPP1
Corresponding Author:	Anabelle Decottignies Catholic University of Louvain Brussels, BELGIUM
First Author:	Harikleia Episkopou
Order of Authors:	Harikleia Episkopou
	Aurélie Diman
	Eloïse Claude
	Nikenza Viceconte
	Anabelle Decottignies
Abstract:	A significant fraction (~10%) of cancer cells maintain their telomere length via a telomerase-independent mechanism known as Alternative Lengthening of Telomeres (ALT). Currently, there are no known molecular, ALT-specific, therapeutic target. We have identified TSPYL5 (Testis Specific Y-encoded-Like Protein 5) as a PML body component, co-localizing with ALT telomeres and critical for ALT+ cell viability. TSPYL5 was described as an inhibitor of the USP7 deubiquitinase. We report that TSPYL5 prevents the poly-ubiquitination of POT1 – a shelterin component – and protects POT1 from proteasomal degradation, exclusively in ALT+ cells. USP7 depletion rescued POT1 poly-ubiquitination and loss, suggesting that the deubiquitinase activates POT1 E3 ubiquitin ligase(s). Similarly, PML depletion suppressed POT1 poly-ubiquitination, suggesting an interplay between USP7 and PML to trigger POT1 degradation in TSPYL5-depleted ALT+ cells. We demonstrate that ALT telomeres need to be protected from POT1 degradation in ALT-associated PML bodies, and identify TSPYL5 as a ALT+ cancer-specific therapeutic target.
Suggested Reviewers:	Roger Reddel, Professor Director of Children's Medical Research Institute (CMRI), CMRI RReddel@cmri.org.au Discovered the ALT mechanism in human cancer cells and still actively working in this field
	Eros Lazzerini Denchi, PhD Stadtman Investigator, NIH eros.lazzerinidenchi@nih.gov Specialist in telomere, DNA damage response at telomeres and POT1
	Brian Luke, Professor Adjunct Director, Institute of Molecular Biology (IMB), Mainz, Institute of Molecular Biology (IMB), Mainz b.luke@imb-mainz.de Specialist in telomere biology and DNA damage response at telomeres
	Roger A. Greenberg, PhD Director of Basic Science, Basser Research Center for BRCA, The Perelman School of Medicine at the University of Pennsylvania rogergr@pennmedicine.upenn.edu Specialist in homologous recombination and the ALT mechanism

Powered by Editorial Manager® and ProduXion Manager® from Aries Systems Corporation

Opposed Reviewers:	Dirk Hockemeyer Assistant Professor of Cell and Developmental Biology, UC Berkeley hockemeyer@berkeley.edu Conflict of interest
Additional Information:	
Question	**Response**
If your original submission was submitted on or after Aug 20th, 2016, we ask that you deposit original imaging data as outlined in our Instructions to Authors and in these detailed Instructions. Please choose all that apply.	I would like to publish this Mendeley Dataset alongside the paper and have included the DOI URL in the “Deposited Data” section of the Key Resources Table.

Powered by Editorial Manager® and ProduXion Manager® from Aries Systems Corporation

- Regarding the new Table S1: (1) the table should be referenced in the main document. After the STAR method section, you need to add a section called "Supplementary Excel Table legends" and add "Table S1. Oligonucleotides used in this study, Related to STAR Methods.", (2) you also need to remove the oligonucleotides from the Key Resources Table, and add "see Table S1" under the section called "Oligonucleotides".

This has been fixed.

- Please ensure your Graphical Abstract is an exact square, 1200 x 1200 pixels in dimension at 300 dpi without needing to be cropped.

This has been fixed.

- We ask that declarations stated on the form, including declarations that confirm there are no competing interests, be included in the manuscript in a section titled "Declaration of Interests" after the Author Contributions section. Please see the form for additional details.

This has been fixed.

Thanks and best wishes,
Anabelle

- Regarding the new Table S1: (1) the table should be referenced in the main document. After the STAR method section, you need to add a section called "Supplementary Excel Table legends" and add "Table S1. Oligonucleotides used in this study, Related to STAR Methods.", (2) you also need to remove the oligonucleotides from the Key Resources Table, and add "see Table S1" under the section called "Oligonucleotides".

This has been fixed.

- Please ensure your Graphical Abstract is an exact square, 1200 x 1200 pixels in dimension at 300 dpi without needing to be cropped.

This has been fixed.

- We ask that declarations stated on the form, including declarations that confirm there are no competing interests, be included in the manuscript in a section titled "Declaration of Interests" after the Author Contributions section. Please see the form for additional details.

This has been fixed.

Thanks and best wishes,
Anabelle

Click here to access/download
Graphical Abstract
Graphical Abstract-Episkopou-16 May.pdf

TSPYL5 depletion induces specific death of ALT cells through USP7-dependent proteasomal degradation of POT1

Harikleia Episkopou[1,†], Aurélie Diman[1,†#], Eloïse Claude[1], Nikenza Viceconte[1,‡], Anabelle Decottignies[1,*]

[1]Genetic and Epigenetic Alterations of Genomes, de Duve Institute, Faculty of Pharmacy and Biomedical Sciences, Université catholique de Louvain, Brussels, 1200, Belgium.

*Lead contact: anabelle.decottignies@uclouvain.be

†equal contributions

#current address: Department of Microbiology and Molecular Medicine, University Medical Centre, Geneva 4, 1211, Switzerland.

‡current address: Quantitative Proteomics, Institute of Molecular Biology gGmbH, Mainz, 55131, Germany.

Summary

A significant fraction (~10%) of cancer cells maintain their telomere length via a telomerase-independent mechanism known as Alternative Lengthening of Telomeres (ALT). Currently, there are no known molecular, ALT-specific, therapeutic target. We have identified TSPYL5 (Testis Specific Y-encoded-Like Protein 5) as a PML body component, co-localizing with ALT telomeres and critical for ALT$^+$ cell viability. TSPYL5 was described as an inhibitor of the USP7 deubiquitinase. We report that TSPYL5 prevents the poly-ubiquitination of POT1 – a shelterin component – and protects POT1 from proteasomal degradation, exclusively in ALT$^+$ cells. USP7 depletion rescued POT1 poly-ubiquitination and loss, suggesting that the deubiquitinase activates POT1 E3

ubiquitin ligase(s). Similarly, PML depletion suppressed POT1 poly-ubiquitination, suggesting an interplay between USP7 and PML to trigger POT1 degradation in TSPYL5-depleted ALT$^+$ cells. We demonstrate that ALT telomeres need to be protected from POT1 degradation in ALT-associated PML bodies, and identify TSPYL5 as a ALT$^+$ cancer-specific therapeutic target.

Keywords: Testis Specific Y-encoded-Like Protein 5, Alternative mechanism of telomere lengthening, PML body, POT1, USP7, TPP1

Introduction

Telomeres are specialized nucleoprotein structures located at the end of eukaryotic chromosomes and capped by a six-protein complex, called shelterin, consisting of TRF1 (Telomeric Repeat Binding Factor 1), TRF2, TIN2 (TRF1-Interacting Nuclear Protein 2), RAP1 (Repressor/Activator Protein 1 Homolog), TPP1 (TIN2 and POT1-interacting Protein) and POT1 (Protection Of Telomeres 1) (de Lange, 2005).

TRF1 and TRF2 are double-stranded telomeric DNA-binding proteins bridged by TIN2, a protein involved in the recruitment of TPP1-POT1 heterodimer to telomeres. POT1 interaction with cytoplasmic TPP1 is required for the nuclear import of the heterodimer (Liu et al., 2004, Ye et al., 2004, Chen et al., 2007). POT1 binds the telomeric G-rich 3'-overhang to prevent RPA binding and activation of ATR, the DNA damage response pathway kinase (Denchi et al., 2007, Gong and de Lange, 2010). POT1 plays additional important roles in regulating telomerase – access and activity – at telomeres (Liu et al., 2004, Loayza and de Lange, 2003, Wang et al., 2007).

Although telomere maintenance mechanisms (TMM) are not activated in all cancer cells (Viceconte et al., 2017, Dagg et al., 2017), about 80-85% of human tumors display telomerase activity, while 10-15% of human tumors, mostly of mesenchymal origin, maintain telomeres by a telomerase-independent mechanism referred to as Alternative Lengthening of Telomeres (ALT) (Cesare and Reddel, 2010). ALT telomeres are maintained through homologous recombination, a feature resulting from the acquisition of numerous genetic and epigenetic alterations, such as the frequent loss of

the chromatin remodeling factor ATRX (Pickett and Reddel, 2015). Several unusual characteristics are associated with ALT telomeres, including a highly heterogeneous length, a reduced nucleosome density and the presence of variant telomeric repeats (Pickett and Reddel, 2015, Episkopou et al., 2014). Another feature of ALT telomeres is their frequent clustering within Promyelocytic Leukemia (PML) nuclear bodies in the so-called ALT-associated PML bodies (APBs). APBs are found exclusively in ALT$^+$ cells and play a direct role in telomere recombination by bringing together chromosome ends and recombination proteins (Draskovic et al., 2009, Osterwald et al., 2015). However, the exact nature of the cellular events driving the clustering of ALT telomeres within PML bodies is still unclear; but likely involves post-translational modifications of shelterin proteins (Potts and Yu, 2007, Osterwald et al., 2015).

Identifying ALT-specific therapeutic targets, though a major challenge, offers interesting perspectives for targeted cancer therapies, since this TMM is not active in normal cells. In this study, through a transcriptomic approach in a model of cellular hybrids, we have identified TSPYL5 as a previously unrecognized PML body component and a potential therapeutic target candidate. We show that TSPYL5 co-localizes with ALT telomeres and is required to maintain POT1 protein levels in ALT$^+$ cells. Strikingly, TSPYL5 expression is absolutely critical for ALT$^+$ cell viability. Previously, TSPYL5 has been described as an inhibitor of the USP7 (Ubiquitin Specific Peptidase 7) deubiquitinase (DUB) (Epping et al., 2011). Among others, USP7 targets include the shelterin component TPP1 (Zemp and Lingner, 2014) and various E3 ligases. Ironically, USP7 interaction with the E3 ligases leads to their protection from auto-ubiquitination and degradation, thus effectively turning the DUB/E3 interacting proteins into an active E3 ligase complex (Kim and Sixma, 2017). Our data indicate that, in ALT$^+$ cells, TSPYL5 is required to prevent the USP7-dependent poly-ubiquitination of POT1 and its subsequent proteasomal degradation. The sensitivity of ALT$^+$ cells to TSPYL5 depletion likely results from the co-localization of ALT telomeres with PML bodies as co-depleting PML in ALT$^+$ cells lacking TSPYL5 suppresses POT1 poly-ubiquitination and degradation. Altogether, our study unravels the necessity for protection of ALT telomeres – that co-localize abnormally with PML bodies – and identifies TSPYL5 as a promising target for ALT$^+$ cancer therapy.

Results

High *TSPYL5* expression co-segregates with ALT$^+$ phenotype in cellular hybrids

Fusion between telomerase-expressing (TEL$^+$) and ALT$^+$ cells generates unstable cellular hybrids, wherein one of the two original TMMs must be repressed, to maintain only a single active mechanism (Bower et al., 2012). This implies random elimination of supernumerary chromosomes, followed by natural selection processes. We (Episkopou et al., 2014), and others (Bower et al., 2012), have previously relied on hybrids to identify genotypic and/or phenotypic alterations that co-segregate with one of the two TMM. Previously, we fused two post-crisis survivors derived from SV40T antigen-mediated *in vitro* immortalization of IMR90 fetal lung fibroblasts, SW39/TEL$^+$ and IMRB/ALT$^+$ cell lines, and isolated SI24 – an ALT$^+$ hybrid (Episkopou et al., 2014). We repeated the hybridization and obtained 8G12 and 7F10 as two new ALT$^+$ hybrids based on heterogeneous telomere length (Fig. 1A), presence of APBs (Fig. 1B) and lack of both telomerase activity and ATRX protein (Fig. S1A-B). On the contrary, the 6C3 hybrid displayed characteristic TEL$^+$ properties, similarly to our first generation hybrids: SI14 (Episkopou et al., 2014) and SI27 (Fig. 1A-C, Fig. S1A-B). To search for genes with up-regulated expression in ALT$^+$ hybrids, we performed a transcriptomic microarray analysis of SI14/TEL$^+$ and SI24/ALT$^+$ cells. Among the ten most up-regulated genes, we selected *TSPYL5* because of its established interaction with USP7 (Epping et al., 2011), a deubiquitinating enzyme previously reported to interact with TPP1 (Zemp and Lingner, 2014). Furthermore, TSPYL5 is known to compete with p53 for binding to USP7, in cancer cells treated with DNA damaging drugs, leading to proteasomal degradation of poly-ubiquitinated p53 (Epping et al., 2011).

The up-regulation of *TSPYL5* transcripts was confirmed in all four ALT$^+$ cell lines (P=0.017) (Fig. 1D) and TSPYL5 protein levels mirrored their respective mRNA profiles (Fig. 1E). Since *TSPYL5* gene expression is regulated by DNA methylation of the promoter (Gallagher et al., 2005), the slightly increased expression of *TSPYL5* gene in

TEL$^+$ hybrids compared to SW39/TEL$^+$ parental cell line (Fig. 1D) likely results from the partial demethylation of genomic DNA during the hybridization process.

We then expanded our analysis to additional TEL$^+$ (MG63, HT1080, 143B) and ALT$^+$ (U2OS, SaOS-2) sarcoma-derived cell lines. We also included VA13/ALT$^+$ SV40T-immortalized WI38 fetal lung fibroblasts and non-immortalized HFF2 normal foreskin fibroblasts. *TSPYL5* mRNA expression correlated with *TSPYL5* gene DNA methylation levels but not with TMM in these cell lines (Fig. 1F-G), suggesting that the up-regulation of *TSPYL5* mRNA in ALT$^+$ hybrids could be occurring through the positive selection pressure for efficient establishment of ALT mechanism in hybrids that initially possessed both TMM.

TSPYL5 is a PML body component that co-localizes with ALT telomeres

Currently, the human *TSPYL5* gene, identified in 1998 (Vogel et al., 1998), is functionally uncharacterized. Although members of the TSPY-like family are characterized by the presence of a NAP (Nucleosome Assembly Protein) domain involved in histone binding, the intracellular localization of TSPYL5 has not been studied yet.

Immunofluorescence analysis of TSPYL5, in combination with FISH against telomeres, revealed a co-localization of TSPYL5 with telomeres of ALT$^+$, but not TEL$^+$, cells (Fig. 1H-I). Importantly, even though the TSPYL5 expression levels were low in VA13/ALT$^+$ cells, about 30% of telomeres were showing TSPYL5 staining (Fig. 1H-I). As TSPYL5 staining showed a punctate pattern in both TEL$^+$ and ALT$^+$ cell lines, but co-localized only with ALT telomeres, we asked whether TSPYL5 might be localized to PML bodies. Immunofluorescence analysis of TEL$^+$ cells revealed a co-localization between TSPYL5 and PML bodies (Fig. 1J). To test whether the co-localization between ALT telomeres and TSPYL5 was merely reflecting their association with PML bodies, we performed a triple staining of telomeres, TSPYL5 and PML in SI24, U2OS and VA13 ALT$^+$ cell lines (Fig. 1K). Interestingly, we found that, although more than 99% of TSPYL5-stained telomeres were also associated with PML bodies in the VA13/ALT$^+$ cell line – which displays the highest frequency of PML-associated telomeres – a fraction of TSPYL5-associated telomeres did not localize to PML bodies

in SI24/ALT$^+$ and U2OS/ALT$^+$ cells (Fig. 1L). In stark contrast, occasionally, when telomeres of TEL$^+$ cells did co-localize with PML bodies, the TSPYL5 and FISH signals did not display a perfect overlap (Fig. 1M).

Thus, we conclude that TSPYL5, regardless of its expression level in the cell, is a component of ALT telomeres. We propose that the presence of TSPYL5 at ALT telomeres is linked not only to their association, event transiently, with PML bodies, but also to additional features of ALT telomeres.

TSPYL5 is required to maintain viability of ALT$^+$ cells

Having shown that TSPYL5 co-localizes with ALT telomeres, we next examined whether TSPYL5 may protect ALT$^+$ cells from telomere dysfunction which, as reported previously, can cause death of human cells with compromised p53-dependent response (Karlseder et al., 1999).

To this end, we tested the impact of *TSPYL5* depletion in TEL$^+$ (SW39 and SI27 with, respectively, low and intermediate *TSPYL5* expression level) and ALT$^+$ (IMRB, SI24 and 8G12) SV40T-immortalized fibroblasts. Cells were transfected with either non-targeting siRNAs against Luciferase gene (siLuci) or with siRNAs directed against TSPYL5 (siTSPYL5) (Fig. S2A). We observed a severe and significant reduction in the number of metabolically active cells following TSPYL5 depletion, exclusively in the ALT$^+$ cells, and not in the TEL$^+$ cells (Fig. 2A) (P<0.01). Annexin V/PI staining revealed a significant increase in the number of dead cells following TSPYL5 depletion in the SI24/ALT$^+$ cells (P<0.0001), but not in SI27/TEL$^+$ cells (Fig. 2B-C). The impact of *TSPYL5* depletion on SI24/ALT$^+$ cell viability was comparable to that of cells treated with the DNA damaging agent etoposide (Fig. S2B).

Importantly, depletion of TSPYL5 reduced the viability of U2OS, SaOS-2 and VA13 ALT$^+$ cell lines, independently of the TSPYL5 expression level, while no effect on the proliferation of TEL$^+$ cells was observed (Fig. 2D). Morphological observation of the cells unambiguously confirmed that U2OS/ALT$^+$, but not HT1080/ TEL$^+$ cells were profoundly affected by TSPYL5 depletion (Fig. S3). Furthermore, TSPYL5 depletion did not affect the proliferation of HFF2 normal foreskin fibroblasts that lack any TMM,

reinforcing the idea that TSPYL5 is specifically required to maintain viability of ALT$^+$ cells (Fig. 2D).

TSPYL5 is required to maintain POT1 protein levels in ALT$^+$ cells

The association of TSPYL5 with ALT telomeres, and its crucial role in maintaining ALT$^+$ cell viability, suggested an important function for TSPYL5 at ALT telomeres. Therefore, we asked whether TSPYL5 depletion could lead to dysfunctional telomeres in ALT$^+$ cells. Quantification of TIF (Telomere dysfunction Induced Foci), based on the co-localization of 53BP1 and telomeres, revealed a significant increase of dysfunctional telomeres in TSPYL5-depleted SI24/ALT$^+$ cells, with at least 50% of the cells displaying three or more TIF (Fig. 3A-B). Shelterin component analysis indicated no discernable reduction in protein levels of RAP1, TRF1, TPP1 and TRF2, but a drastic down-regulation of POT1 – by more than 60% – in both SI24/ALT$^+$ and 8G12/ALT$^+$ cell lines (P<0.001 and P<0.005 respectively), but not in SI27/TEL$^+$ cell line (Fig. 3C-D). POT1 was lost from both the cytoplasmic and the chromatin fractions of TSPYL5-depleted SI24/ALT$^+$ cells (Fig. 3E), independently of any discernible reduction in *POT1* mRNA (Fig. S4) or mutation in the *POT1* coding sequence. Visualization of POT1 protein in combination with telomeric FISH further confirmed the loss of POT1 from telomeres of TSPYL5-depleted SI24/ALT$^+$ cells (Fig. 3F). Since the telomeric association of TPP1 was not reduced by *TSPYL5* knock-down (Fig. 3F-G), the observed POT1 loss in SI24/ALT$^+$ is not a consequence of defective TPP1 recruitment.

Telomere dysfunction was also observed in U2OS/ALT$^+$, but not in HT1080/TEL$^+$ sarcoma cell line (Fig. 3H-I), and was associated with POT1 loss (Fig. 3J). We confirmed loss of POT1 protein in TSPYL5-depleted SaOS-2/ALT$^+$ and VA13/ALT$^+$ cell lines (Fig. 3J) and in U2OS/ALT$^+$ and SI24/ALT$^+$ cells treated with a second siRNA against *TSPYL5* (Fig. S5). In accordance with the cell viability measurements, the levels of POT1 were not affected in MG63/TEL$^+$, 143B/TEL$^+$ cancer cell lines or HFF2 normal foreskin fibroblasts depleted of TSPYL5 (Fig. 3J).

Collectively, these data show that TSPYL5 is specifically required to maintain POT1 protein in ALT$^+$ cells.

TSPYL5 is required to protect POT1 from proteasomal degradation in ALT$^+$ cells

The loss of POT1 protein upon TSPYL5 knock-down in ALT$^+$ cells was not associated with a reduction in mRNA levels, suggesting that POT1 protein may be proteosomally degraded. In support of the hypothesis that TSPLY5 prevents POT1 proteasomal degradation in ALT$^+$ cells, treating TSPYL5-depleted U2OS/ALT$^+$ cells with a proteasome inhibitor, MG132, rescued POT1 loss (Fig. 4A). Along the same line, TSPYL5 depletion increased the levels of poly-ubiquitinated POT1 (Fig. 4B), suggesting that TSPYL5 protects POT1 from poly-ubiquitination in ALT$^+$ cells. Since TSPYL5 depletion was associated with a massive loss of POT1, we next determined whether this was the cause of the observed cell death. To do this, we transiently overexpressed Myc-POT1 in U2OS/ALT$^+$ depleted of TSPYL5. Accordingly, we found that Myc-POT1 overexpression rescued POT1 levels, cellular viability and TIF induction (Fig. 4C-G).

Taken together, these data suggest that, in TSPYL5-depleted ALT$^+$ cells, POT1 becomes limiting due to proteasomal degradation, leading to telomere dysfunction and cell death. POT1 depletion experiments show that ALT$^+$ and TEL$^+$ cells display similar loss of viability in the absence of POT1 (Fig. 4H-I), further supporting our observation that POT1 loss only occurs in ALT$^+$ cells depleted from TSPYL5 and is causing cell death.

***USP7* depletion rescues POT1 loss in TSPYL5-depleted ALT$^+$ cells**

To elucidate the mechanisms underlying the proteasome-dependent loss of POT1 in TSPYL5-depleted ALT$^+$ cells, we first tested whether TSPYL5 may directly interact with POT1. However, overexpressed Myc-POT1 protein in U2OS/ALT$^+$ cells failed to co-immunoprecipitate TSPYL5 while TPP1 was successfully pulled-down (Fig. S6A). Thus, we reasoned that TSPYL5 depletion might affect POT1 abundance *via* an indirect mechanism involving other partners.

TSPYL5 and TPP1 have been previously reported to interact with USP7- a deubiquitinating enzyme with multiple targets, including TPP1 itself. We first hypothesized that TPP1 interaction with USP7 may be required to retain POT1 at ALT telomeres and that TSPYL5 may possibly stabilize the USP7-TPP1 complex. If this

were true, USP7 would also be required for POT1 stabilization. However, *USP7* knock-down did not affect POT1 levels, either in SI24/ALT$^+$ or in U2OS/ALT$^+$ cells (Fig. 5A), arguing against the requirement of the TPP1/USP7/TSPYL5 interaction for POT1 maintenance at telomeres. Instead, we hypothesized that TSPYL5 could compete with TPP1 for binding to USP7, similar to the competition model between TSPYL5 and p53 for the N-terminal MATH domain of USP7 (Epping et al., 2011), which is also the domain required for the TPP1/USP7 interaction (Zemp and Lingner, 2014). We reasoned that the TPP1/USP7 interaction could destabilize POT1 and that TSPYL5 would titrate USP7 away from TPP1. In support of this competition model, POT1 loss in TSPYL5-depleted ALT$^+$ cells was rescued by the concomitant depletion of USP7 (Fig. 5A) and TSPYL5 depletion increased the binding of USP7 to TPP1 (Fig. 5B). Simultaneously, USP7 recruitment reduced TPP1 ubiquitination levels (Fig. 5C).

On one hand, TSPYL5 knock-down was associated with POT1 loss and, on the other hand, with a reduction in TPP1 ubiquitination; we next tested whether TPP1 deubiquitination was the cause of POT1 degradation. However, overexpression of the ubiquitination-defective TPP1(10R)-3xHA mutant (Zemp and Lingner, 2014) in U2OS/ALT$^+$ cells did not induce POT1 loss (Fig. 5D-F), ruling out the possibility that TPP1 ubiquitination was required to protect POT1 from proteasomal degradation in ALT$^+$ cells. These observations are in line with the demonstration that ubiquitination of human TPP1 does not regulate POT1 interaction *in vitro* and is not required for telomere protection in TEL$^+$ cells (Zemp and Lingner, 2014).

As a defective interaction between TPP1 and POT1 was recently reported to induce the proteasomal degradation of POT1 (Chen et al., 2017), we next hypothesized that the binding of USP7 protein to the OB domain of TPP1 could be sufficient to destabilize the interaction between POT1 and TPP1. To test that hypothesis, we overexpressed the TPP1 (S132A)-3xHA mutant, unable to bind to USP7 (Zemp and Lingner, 2014), in U2OS/ALT$^+$ cells (Fig. 5G). However, even though the TPP1 mutant was properly localized to telomeres (Fig. 5H), it did not prevent POT1 loss upon TSPYL5 depletion (Fig. 5I). Furthermore, when POT1 loss was prevented by treating cells with MG132 proteasome inhibitor, TPP1/POT1 interaction was not altered (Fig. 5J); arguing against the hypothesis of a destabilized TPP1/POT1 interaction in ALT$^+$

cells lacking TSPYL5. Taken together, these observations suggest that, although USP7 is required for POT1 loss in TSPYL5-depleted ALT$^+$ cells, its recruitment to TPP1 is not the primary cause for POT1 degradation.

We next tested whether USP7 may directly interact with POT1 upon TSPYL5 depletion. However, whether in siLuci or in siTSPYL5 conditions, overexpressed Myc-POT1 protein, in U2OS/ALT$^+$ cells treated with MG132 proteasome inhibitor, failed to co-immunoprecipitate USP7, while TPP1 was successfully pulled-down (Fig. S6B).

Altogether, these data show that the role of USP7 in TSPYL5 depletion-induced POT1 degradation is not mediated by a direct interaction of the DUB with either TPP1 or POT1.

USP7 co-localizes with telomeres in both TEL$^+$ and ALT$^+$ cells

Next, we hypothesized that the ALT$^+$ cell sensitivity to USP7-dependent POT1 loss may result from a distinct abundance and/or intracellular localization of USP7 in these cells. However, USP7 protein levels did not show any consistent difference between TEL$^+$ and ALT$^+$ cells (Fig. 6A). In accordance with the mass spectrometry-based analysis of telomere-bound proteins (Déjardin and Kingston, 2009), USP7 co-localized with a subset of telomeres in both TEL$^+$ and ALT$^+$ cells (Fig. 6B-C). However, we noticed a difference in the telomere-association pattern of USP7: there were more telomere-associated USP7 foci in U2OS/ALT$^+$ and VA13/ALT$^+$ cells than in the other tested cell lines (Fig. 6B-C). Importantly, USP7 still localized to the telomeres of U2OS/ALT$^+$ cells overexpressing the TPP1 (S132A)-3xHA mutant (Fig. 6D), further reinforcing the idea that the negative impact of USP7 on POT1 levels occurs independently of its association with TPP1.

Our observation that the recruitment of USP7 to TPP1 is not responsible for POT1 degradation in TSPYL5-depleted ALT$^+$ cells, together with the detection of a constitutive association of both USP7 and TSPYL5 with ALT telomeres, suggests the possibility of a distinct USP7-dependent mechanism, which gets activated by TSPYL5 depletion from ALT telomeres.

PML is required for the USP7-dependent loss of POT1 in TSPYL5-depleted ALT$^+$ cells

Interestingly, one of the main functions of USP7 is to stabilize the E3 ubiquitin ligases that interact with the DUB through its C-terminal domain (Kim and Sixma, 2017). Thus, we hypothesized that USP7 activation, through TSPYL5 depletion, may stabilize E3 ligase(s) that could, in turn, poly-ubiquitinate POT1. However, since USP7 is telomere-bound in both TEL$^+$ and ALT$^+$ cells, why is POT1 poly-ubiquitination, following TSPYL5 depletion, exclusive to ALT$^+$ cells? One of the main characteristics of ALT telomeres is their co-localization with PML bodies, which are associated with ubiquitination and proteasomal degradation of proteins (Rockel et al., 2005). The PML protein itself interacts with several ubiquitin ligases (Cheng and Kao, 2013). Moreover, USP7 was reported to directly interact with PML proteins I or IV in PML bodies (Sarkari et al., 2011). Hence, we hypothesized that the co-localization of ALT telomeres with PML bodies and/or the exclusive presence of PML protein at ALT telomeres (Déjardin and Kingston, 2009, Garcia-Exposito et al., 2016) may sensitize POT1 to USP7-dependent poly-ubiquitination and degradation in TSPYL5-depleted ALT$^+$ cells. To test this hypothesis, we co-depleted PML and TSPYL5 in ALT$^+$ cells (Fig. 7A).

Strikingly, PML knock-down fully rescued POT1 loss in TSPYL5-depleted SI24/ALT$^+$ cells (siTSPYL5/siPML) and telomeric POT1 was recovered (Fig. 7B-D). Importantly, POT1 rescue was not due to USP7 degradation upon PML and TSPYL5 depletion (Fig. 7E) and USP7 still localized to ALT telomeres in cells lacking either TSPYL5 or PML (Fig. S7). In agreement with a role for USP7 and PML in the E3 ligase-mediated poly-ubiquitination of POT1, depletion of either PML or USP7 completely abolished the poly-ubiquitination of POT1 in TSPYL5-depleted ALT$^+$ cells (Fig. 7F). The observation that damaged telomeres were highly enriched in PML bodies of these cells (Fig. 7G-H) further supported the hypothesis of a PML-dependent degradation of POT1 in TSPYL5-depleted ALT$^+$ cells.

In summary, these data suggest that the localization of ALT telomeres in APBs puts these telomeres at risk by sensitizing cells to USP7- and PML-dependent poly-ubiquitination and degradation of POT1.

Discussion

An estimated 10% of cancer cells achieve cellular immortality through a telomerase-independent alternative mechanism of telomere lengthening. Since the ALT mechanism is unlikely to operate in normal human cells, it presents a lucrative, specific therapeutic target for cancer. While anti-telomerase inhibitors have recently entered clinical trials for hematologic malignancies (Baerlocher et al., 2015; Tefferi et al., 2015) and are being considered for treating non-small cell lung cancer (Frink et al., 2016), no therapeutic drug has been identified to specifically target ALT$^+$ cells. The recombination events observed at ALT$^+$ telomeres appear to operate through homologous recombination-based mechanisms similar to the ones that operate throughout the genome for DNA repair. Hence, even though knock-down of a series of homologous recombination-related genes has been reported to affect ALT$^+$ cell proliferation (Cesare and Reddel, 2010), targeting these genes cannot be viewed as a possible therapeutic option.

Here, through a transcriptomic screen in ALT$^+$ and TEL$^+$ hybrids, we identified TSPYL5 as a previously unidentified target with therapeutic potential against ALT$^+$ cancer cells. We could show that, regardless of the TSPYL5 protein expression levels, *TSPYL5* knock-down induces cell death through the poly-ubiquitination and proteasome-dependent degradation of a key shelterin component- POT1, in ALT$^+$ cells, but not in TEL$^+$ cells nor in non-immortalized fibroblasts. Our observation that TSPYL5-dependent stabilization of POT1 in ALT$^+$ cells operates through USP7 adds to the previously recognized role of TSPYL5 as a competitor for USP7 deubiquitinase towards p53 and, therefore, as an oncogene (Epping et al., 2011). Additional substrates of USP7 have been previously described and include the POT1 interaction partner, TPP1 (Zemp and Lingner, 2014). Previously, USP7 was found to interact with- and to remove ubiquitin moieties from TPP1, but no telomere biology-related function has been assigned to TPP1 ubiquitination (Zemp and Lingner, 2014). Zemp and Lingner convincingly demonstrated that TPP1 ubiquitination is not required for the telomeric localization of human TPP1 and does not regulate its interaction with POT1.

Conversely, Rnf8-dependent ubiquitination of mouse TPP1 appears to be important to keep TPP1 at telomeres (Rai et al., 2011). In agreement with the study by Zemp and Lingner, our data show that TPP1 ubiquitination is not required for TPP1 recruitment to ALT telomeres since, in cells depleted for TSPYL5, TPP1 was deubiquitinated but still localized to telomeres. Moreover, overexpressed ubiquitination-deficient TPP1 (10R) mutant localized to telomeres and, importantly, did not induce POT1 loss, suggesting that TPP1 ubiquitination is not required to keep POT1 at ALT telomeres. Our data further suggest that the recruitment of USP7 to the OB domain of TPP1 does not induce POT1 degradation.

Many of the USP7-interacting proteins and substrates are in fact E3 ubiquitin ligases (Kim and Sixma, 2017). Protection of E3 ubiquitin ligases from auto-ubiquitination and degradation through the USP7 deubiquitinase activity has been well documented for E3 ubiquitin ligases – viral ICP0 (Canning et al., 2004) or human RNF169 (An et al., 2017) – and requires their direct interaction with the C-terminal ubiquitin-like domains of USP7. Additional E3 ligases that interact with – and are regulated by USP7 – include MDM2, TRIM27, RAD18, UHRF1, RING1B or TRIM32 (Kim and Sixma, 2017; Nicklas et al., 2019). Our results indicate that the role of TSPYL5 in keeping POT1 levels in ALT$^+$ cells may be linked to its ability to counteract the USP7-dependent stabilization of yet unidentified E3 ubiquitin ligase(s) able to poly-ubiquitinate POT1 (Fig. 7I). Upon depletion of TSPYL5, USP7, still localized at telomeres, may stabilize an associated ubiquitin ligase and induce POT1 poly-ubiquitination and degradation by the proteasome (Fig. 7I). Interestingly, the ATRX interaction partner- DAXX has been reported to regulate the interplay between USP7 and MDM2 (Tang et al., 2006), suggesting that the loss of ATRX in ALT$^+$ cells may play a role in the USP7-dependent poly-ubiquitination of POT1 by changing DAXX interactions with other partners.

Our results indicate that the USP7-dependent poly-ubiquitination of POT1 requires PML protein and/or other PML body components (Fig. 7I). Along this line, both the N- and the C-terminal parts of USP7 have been reported to interact directly with PML proteins I and IV in PML bodies (Sarkari et al., 2011). It is thus plausible that, in

the absence of TSPYL5, the binding of PML to USP7 may help bringing PML-binding E3 ligases – like RNF4, UHRF1, MDM2 or TRIM27 (Cao et al., 1998; Wei et al., 2003; Cheng and Kao, 2013) – to POT1 (Fig. 7I). Interestingly, several E3 ubiquitin ligases, like MDM2, TRIM27 or UHRF1, bind to both USP7 and PML, further supporting the hypothesis of a cooperation between USP7 and PML at TSPYL5-depleted ALT telomeres. Together with the fact that PML bodies contain many E3 ligases, the identification of POT1's E3 may be complicated by the fact that individual protein substrates can be targeted by multiple E3 ligases (Iconomou and Saunders, 2016). On the other hand, as PML also interacts with DAXX (Salomoni, 2013), it is tempting to speculate that PML and DAXX could collaborate to mediate the USP7-activated poly-ubiquitination of POT1 in TSPYL5-depleted ALT$^+$ cells. Whether the PML protein itself or other components of the PML bodies, whose activity may be lost upon PML knock-down, are involved in USP7-dependent poly-ubiquitination of POT1 is still unknown. Agreeing with a direct role for PML protein in POT1 poly-ubiquitination is the observation that the PML protein appears to be an exclusive constituent of ALT telomeres (Déjardin and Kingston, 2009, Garcia-Exposito et al., 2016). Thus, the association of ALT telomeres with PML bodies, which likely explains the presence of PML protein at ALT telomeres, may put POT1 at risk of poly-ubiquitination and degradation (Fig. 7I). We identify TSPYL5 to be a constitutive component of PML bodies, which may similarly be recruited to ALT telomeres during their association with these subnuclear structures; and thus, protect POT1 from USP7- and PML-dependent poly-ubiquitination. To date, it is still unclear why ALT telomeres associate with PML protein/PML bodies. The absence of ATRX in most ALT$^+$ cells may contribute to APB formation but further work is required to investigate this possibility.

Altogether, our study unveils a unique role for the TSPYL5 PML body-associated component in POT1 maintenance and viability in ALT$^+$ cells. Furthermore, we propose that disruption of the interaction between TSPYL5 and USP7 may provide interesting therapeutic opportunities to specifically induce cell death in ALT$^+$ cancers, with minimal side effects to normal healthy tissues.

Author contributions

H.E., A.Di. and A.De. designed the study, H.E., A.Di., N.V. and E.C. performed and analyzed the experiments and A.De. wrote the manuscript. H.E. and A.Di. contributed equally to the work.

Declaration of Interests.

Authors declare no competing interests.

Acknowledgments

We thank G. Tilman and A. Van Beneden for generating the cellular hybrids and L. Dumoutier and E. Hendrickx for help with microarrays. We are grateful to R. Bernards (NCI, Amsterdam), J. Lingner (EPFL, Lausanne) and T. de Lange (Anderson Center for Cancer Research, Rockefeller University) for sharing reagents. We are indebted to J. Karlseder, N. Arnoult, R. Guerois and M. Raghunandan for critical reading of the manuscript and useful suggestions. **Funding:** This work was supported by grants from the FNRS-Télévie (7.4517.15, 7.6504.16, 7.4519.18) (H.E., A.Di., E.C.), the FNRS (A.De) and the de Duve Institute (N.V.); **Data and materials availability:** All data is available in the main text or the supplementary materials.

Figure legends

Fig. 1. TSPYL5 is highly expressed in ALT$^+$ hybrids and is a PML body component associated with ALT telomeres. (**A**) Southern blot analysis of telomeres. (**B**) Representative images of TRF2 (green) and PML (red) staining. Bar scale, 10 μm. (**C**) Summary of parental cell lines and hybrids. (**D**) *TSPYL5* mRNA expression, normalized to *ACTB* mRNA and to SW39/TEL$^+$. *n*=3 RNA extractions; mean±SEM, two-tailed unpaired *t*-test. (**E**) Western blot analysis of TSPYL5. (**F**) *TSPYL5* mRNA expression in TEL$^+$ and ALT$^+$ sarcoma cell lines, VA13 ALT$^+$ SV40T-immortalized fibroblasts and HFF2 primary foreskin fibroblasts. Mean±SEM. (**G**) Methylation-specific PCR on

TSPYL5 promoter. Upper panel, methylated; lower panel, unmethylated. (**H**) Representative images of telomeres (red FISH probe) and TSPYL5 (green) staining. Bar scale, 10 μm. (**I**) Quantification of co-localization events between telomeres and TSPYL5, normalized to telomere number, mean±SEM, two-tailed unpaired *t*-tests. (**J**) Representative images of TSPYL5 (green) and PML (cyan) staining. Bar scale, 10 μm. (**K**) Representative images of telomeres (red FISH probe), TSPYL5 (green) and PML (cyan) staining. Bar scale, 10 μm. (**L**) Quantification of co-localization events between telomeres and PML (normalized to telomere number) and between PML, TSPYL5 and telomeres (normalized to the number of TSPYL5-associated telomeres). (**M**) Magnifications of (**K**). See also Figure S1.

Fig. 2. TSPYL5 is required to maintain cellular viability in a variety of ALT$^+$ cell lines. (**A**) Metabolically active cells upon treatment with siTSPYL5 for 6 days, normalized to siLuci-treated cells. 3-4 independent measurements; mean±SEM, two-tailed unpaired *t*-tests. (**B**) Representative FACS analyses of Annexin V/FITC staining in SI24/ALT$^+$ and SI27/TEL$^+$ cells: untreated (Mock), transfected with either siLuci or siTSPYL5 for 3 days. 10,000 events were recorded. (**C**) Quantification of **(B)** from triplicates, after normalization to siLuci-treated cells. Mean±SEM, two-tailed unpaired *t*-tests. (**D**) Same as **(A)** in TEL$^+$ and ALT$^+$ sarcoma cell lines, VA13 ALT$^+$ SV40T-immortalized fibroblasts and HFF2 primary foreskin fibroblasts. Mean±SEM, two-tailed unpaired *t*-tests. See also Figures S2-S3.

Fig. 3. TSPYL5 is required to maintain POT1 protein levels and telomeric integrity in ALT$^+$ cells. (**A**) Representative images of TIF detection in cells treated with siLuci or siTSPYL5 for 4 days. Telomeres: FISH probe (red), DNA damage: 53BP1 antibody (green). Bar scale, 5 μm. Arrowheads indicate TIF. (**B**) Quantification of (**A**) from triplicates. TIF number/nucleus: 0 to 2 (black), 3 to 5 (blue) or >5 (orange). 60-100 nuclei/experiment; mean±SEM, two-tailed unpaired *t*-tests. (**C**) Impact of *TSPYL5* knock-down on shelterin proteins after 3 days. Control cells were transfected with siLuci. (**D**) Quantification of (**C**) from triplicates, normalization to ACTB and to siLuci-treated cells. Mean±SEM, two-tailed unpaired *t*-tests. (**E**) POT1 protein levels in whole

cell extracts (WCE), cytoplasm (Cytopl), nucleoplasm (Nucleopl) and chromatin (Chrom) from siTSPYL5-treated SI24/ALT$^+$ cells. H3 histone was probed to control for chromatin enrichment and GAPDH is a cytoplasmic marker. Control cells were transfected with siLuci. (**F**) Representative images of POT1 and TPP1 detection (green) at telomeres of SI24/ALT$^+$ cells transfected with either siLuci or siTSPYL5 for 3 days. Telomeres: FISH probe (red). Bar scale, 5 μm. (**G**) Quantification of (**F**). 500-750 telomeric signals/condition. Mean±SEM, two-tailed unpaired *t*-tests. (**H**) Same as (**A**) in HT1080/TEL$^+$ and U2OS/ALT$^+$ cell lines. Bar scale, 10 μm. Arrowheads indicate TIF. (**I**) Quantification of (**E**) from triplicates. TIF number/nucleus: 0 to 2 (black), 3 to 5 (blue) or >5 (orange). 50-60 nuclei/experiment. Mean±SEM, two-tailed unpaired *t*-tests. (**J**) POT1 protein levels upon *TSPYL5* knock-down (3 days). Control cells were transfected with siLuci. A longer exposure of the membrane is shown to account for the differences in TSPYL5 expression. POT1/ACTB ratios (normalized to siLuci) are indicated below. See also Figures S4-S5.

Fig. 4. POT1 overexpression rescues telomeric defects and cell death in TSPYL5-depleted ALT$^+$ cells experiencing proteasome-dependent degradation of POT1. (**A**) POT1 protein levels upon *TSPYL5* knock-down (3 days) in U2OS/ALT$^+$ cells treated or not with 10 μM MG132 for 6 hours. Control cells were transfected with siLuci. (**B**) POT1 ubiquitination in U2OS/ALT$^+$ cells transiently transfected with Myc-POT1 and HA-Ubiquitin plasmids for 2 days. Immunoprecipitation: α-Myc; WB: α-POT1 or α-HA. When indicated, cells were treated with 10 μM MG132 for 6 hours. (**C**) POT1 protein levels in U2OS/ALT$^+$ cells transfected with control or Myc-POT1 plasmid and either siLuci or siTSPYL5 for 3 days. (**D**) Metabolically active cells in U2OS/ALT$^+$ treated as indicated for 6 days. Data from triplicates, normalized to siLuci-treated cells transfected with the control plasmid. Mean±SEM, two-tailed unpaired *t*-tests. (**E**) Representative pictures of U2OS/ALT$^+$ cells treated as indicated. Bar scale, 50 μm. (**F**) Representative images of TIF detection in U2OS/ALT$^+$ cells transfected with control or Myc-POT1 plasmid and either siLuci or siTSPYL5 for 4 days. Telomeres: FISH probe (red), DNA damage: 53BP1 antibody (green). Bar scale, 10 μm. Arrowheads indicate TIF. (**G**) Quantification

of (**F**) from triplicates. TIF number/nucleus: 0 to 2 (black), 3 to 5 (blue) or >5 (orange). 50-60 nuclei/experiment. Mean±SEM, two-tailed unpaired *t*-tests. (**H**) POT1 protein levels in the indicated cell lines treated with either siLuci or siPOT1. (**I**) Metabolically active cells upon treatment with siPOT1 for 6 days. Data from triplicates, normalized to siLuci-treated cells. Mean±SEM.

Fig. 5. The recruitment of USP7 to TPP1 in TSPYL5-depleted ALT$^+$ cells is not responsible for POT1 degradation. (**A**) POT1 and TPP1 protein levels in SI24/ALT$^+$ and U2OS/ALT$^+$ cell lines transfected with either siLuci, siTSPYL5, siUSP7 or a combination of both siTSPYL5 and siUSP7 for 3 days. (**B**) U2OS/ALT$^+$ cells were transfected with either siLuci or siTSPYL5 for a total of 3 days and transiently transfected with FLAG-TPP1 plasmid for 2 days. IP: α-Flag antibody. WB: α-USP7 (normal or longer exposition) and α-TPP1. Input fractions are shown on the left panel with ACTB detection as loading control. (**C**) U2OS/ALT$^+$ cells were transfected with either siLuci or siTSPYL5 for 3 days and transiently transfected with 3xFLAG-TPP1 and His-hUbi plasmids for 2 days. Ubiquitinated proteins, bound onto Ni-NTA agarose beads, were eluted and analyzed using a TPP1 antibody. (**D**) U2OS/ALT$^+$ cells, stably transfected with either TPP1(WT)-3xHA (clone 3D5) or non-ubiquitinable TPP1(10R)-3xHA (clone 1A7), were analyzed by immunofluorescence using α-HA antibody (green). Telomeres were detected with a FISH probe (red). Bar scale, 10 μm. (**E**) TPP1(WT or 10R)-3xHA and POT1 protein levels in the stable cell lines described in (**D**). (**F**) Representative images of telomeres (red FISH probe) and POT1 (green) staining in the stable cell lines described in (**D**). Note that, because of the low POT1 expression in U2OS/ALT$^+$ cells, staining is faint. Bar scale, 10 μm. (**G**) TPP1 protein levels in U2OS/ALT$^+$ cells, stably transfected with either TPP1(WT)-3xHA (clone 3D5) or USP7 binding-defective TPP1(S132A)-3xHA (clone 2F11). Non-transfected U2OS/ALT$^+$ cells are shown in the first lane (-). (**H**) Immunofluorescence analysis using α-HA antibody (green) in the 2F11 clone described in (**G**). Telomeres were detected with a FISH probe (red). Bar scale, 10 μm. (**I**) POT1 protein levels in cell extracts from two independent clones of U2OS/ALT$^+$ cells stably transfected with TPP1(S132A)-3xHA (clones 2C2 and 2F11) and transiently transfected with either siLuci or siTSPYL5 for 3 days. (**J**)

SI24/ALT$^+$ cells, stably transfected with 3xFLAG-TPP1, were transiently transfected with either siLuci or siTSPYL5 for 3 days and 10 μM MG132 were added for the last 6 hours. Immunoprecipitation was performed with α-FLAG antibody. Co-immunoporecipitated proteins were analyzed using α-POT1 and α-TPP1 antibodies. See also Figure S6.

Fig. 6. USP7 co-localizes with telomeres in TEL$^+$ and ALT$^+$ cell lines. (**A**) USP7 protein levels in cell extracts. (**B**) Representative images of telomeres (red FISH probe) and USP7 (green) staining. Bar scale, 10 μm. (**C**) Quantification of co-localization events between telomeres and USP7 (normalized to telomere number). Mean±SEM. (**D**) Representative images of telomeres (red FISH probe) and USP7 (green) staining in U2OS/ALT$^+$ cells stably transfected with TPP1(S132A)-3xHA (clone 2F11). Bar scale, 10 μm.

Fig. 7. Knocking-down PML rescues POT1 loss in TSPYL5-depleted ALT$^+$ cells. (**A**) Representative images of telomeres (red FISH probe) and PML (cyan) staining in SI24/ALT$^+$ cells transfected with either siLuci, siTSPYL5, siPML or siTSPYL5+siPML for 3 days. Dotted lines delineate the nucleus. Bar scale, 10 μm. (**B**) Representative images of telomeres (red FISH probe) and POT1 (green) staining in SI24/ALT$^+$ cells transfected as detailed in (**A**). Bar scale, 10 μm. (**C**) POT1 protein levels in cells treated as detailed in (**A**). (**D**) Quantification of (**C**) from triplicates, after normalization to ACTB and to siLuci-treated cells. Mean±SEM, two-tailed unpaired *t*-tests. (**E**) USP7 protein levels in cells treated as detailed in (**A**). (**F**) U2OS/ALT$^+$ cells were transfected with the indicated siRNAs for 3 days and transiently transfected with Myc-POT1 and HA-Ubiquitin plasmids for 2 days. When indicated, cells were treated with 10 μM MG132 for 6 hours. Immunoprecipitation: α-Myc; WB: α-POT1. (**G**) TIF detection in SI24/ALT$^+$ after siTSPYL5 treatment for 4 days. Telomeres: FISH probe (red), DNA damage: 53BP1 (green) and PML bodies: PML (cyan). DNA was stained with DAPI. Bar scale, 10 μm. White arrowheads indicate telomeres co-localizing with 53BP1 (TIF) and PML; yellow arrowheads indicate telomeres co-localizing with 53BP1 but not with PML. (**H**) Quantification of (**G**) in 9 nuclei. Black bars indicate, for each nucleus, the frequency of

telomeres co-localizing with PML staining (APB). Grey bars indicate the frequency of TIF co-localizing with PML bodies in each nucleus. (**I**) Proposed model. In ALT$^+$ cells, telomeres localize in APBs, and interact with USP7, TSPYL5 and PML proteins. TSPYL5 inhibits USP7 deubiquitinase activity towards its substrates that include TPP1 and possible E3 ubiquitin ligase(s). Upon TSPYL5 depletion, USP7 is recruited to and deubiquitinates TPP1. Based on the reported ability of USP7 DUB to stabilize and activate E3 ligases (Kim and Sixma, 2017), we hypothesize that, in conjunction with PML protein and/or PML body, TSPYL5-free USP7 may activate POT1 E3 ligase(s) and trigger its poly-ubiquitination and proteasomal degradation, leading to cell death. See also Figure S7.

STAR Methods section

Contact for Reagent and Resource Sharing

Further information and requests for resources and reagents should be directed to and will be fulfilled by Prof. Anabelle Decottignies, the Lead Contact: anabelle.decottignies@uclouvain.be

Experimental Model and Subject Details

SW39/TEL$^+$ (Genet^R) (kindly provided by W. Wright, UT Southwestern, Dallas, USA) and IMRB/ALT$^+$ (Coriell Institute for medical Research, New Jersey, USA) cell lines derived from IMR90 human female fetal lung fibroblasts were described previously (Tilman et al., 2009). Before hybridization, IMRB/ALT$^+$ cells were transfected with pBABE::Hygro plasmid (Tilman et al., 2009). Cellular hybridization between SW39/TEL$^+$ Genet^R and IMRB/ALT$^+$ Hygro^R was obtained through the procedure described in Episkopou et al. (2014). Briefly, 2 million of cells from the first parental cell line were seeded in a T75 flask. Four hours later, 2 million of cells from the second parental cell line were seeded in the same flask. Four hours later, cells were covered with the hybridization solution (47% PEG 4000, 10% DMSO in serum-free MEM) for 1 minute and then directly washed 3 times with 10% DMSO in serum-free MEM before overnight

incubation in full medium. Hybrids were then selected with 0.2 mg/ml hygromycin B (Sigma-Aldrich) and 2 mg/ml geneticin (MP Biomedicals) for 2 weeks before sub-cloning. Two independent cellular hybridizations were performed: the 1st hybridization was described in Episkopou et al. (2014) and the second one was performed in this study. SI14/TEL$^+$, SI27/TEL$^+$ and SI24/ALT$^+$ hybrids result from the 1st hybridization; 6C3/TEL$^+$, 8G12/ALT$^+$ and 7F10/ALT$^+$ were generated during the 2nd hybridization.

VA13/ALT$^+$ are SV40T immortalized human female fetal lung fibroblasts (kindly provided by J.A. Londoño-Vallejo, Curie Institute, Paris, France) and HFF2 cells (ATCC, Rockville, USA) are normal human male foreskin fibroblasts. All the above cell lines were grown at 37°C in EMEM supplemented with 10% FBS (Gibco), 1% NEAA (Gibco) and 1% penicillin/streptomycin (Lonza). U2OS/ALT$^+$ (female), SaOS-2/ALT$^+$ (female), MG63/TEL$^+$ (male) (Tilman et al., 2009) and 143B/TEL$^+$ (female) (Coriell Institute for medical Research, New Jersey, USA) osteosarcoma cell lines were grown at 37°C in DMEM (Lonza) supplemented with 10% FBS (Gibco), 1% glutamine (Gibco) and 1% penicillin/streptomycin (Lonza). HT1080/TEL$^+$ (male) fibrosarcoma cell line, kindly provided by J. Lingner (EPFL, Lausanne, Switzerland) was grown at 37°C in IMDM (Lonza) supplemented with 10% FBS (Gibco) and 1% penicillin/streptomycin (Lonza). Cell lines have not been authenticated.

Method Details

Transcriptomic analysis

The transcriptomic analysis was performed on RNA extracted from SI14/TEL$^+$ and SI24/ALT$^+$ hybrids using Affymetrix GeneChip® Human Transcriptome Array 2.0 (ThermoFisher Scientific). Whole transcripts were amplified from 250 ng of total RNA and converted into single-stranded DNA using the GeneChIP® WT PLUS Reagent kit (ThermoFisher Scientific). 5.5 μg DNA were fragmented, labeled and hybridized on the array. Affymetrix Bi-weight average signals were analyzed with Excel to identify candidate genes with up-regulation in SI24/ALT$^+$ hybrid.

Transfections

Transfections with siRNAs were performed using Lipofectamine 2000 (ThermoFisher Scientific) according to the manufacturer's instructions. For most

experiments, cells were collected after 3 days of siRNA treatment. For cell viability experiments, cells were transfected again with siRNAs after 3 days and left in culture for another 3 days. siRNAs are listed in the Key Resources Table. For plasmid transfections, we used PEI 25K reagent (Key Resources Table). Cells were seeded in 6-well plates with a density of 0.3 million cells/well and incubated for 24 h before transfection. Per well, 2 μg of plasmid and 8 μl of 1 mg/ml PEI stock solution were mixed in 200 μl of serum-free medium and incubated at RT for 20 min before incubation with the cells for 6 h in 1.8 ml medium supplemented with 10% FBS. After the 6 h incubation, the medium was discarded and replaced by fresh medium supplemented with 10% FBS. Plasmids for transfections are listed in the Key Resources Table.

Cell treatments

For proteasome inhibition, cells were treated for the indicated time points with MG132 (Sigma-Aldrich), to a final concentration of 10 μM. Control cells were treated with DMSO (Sigma-Aldrich). For protein stability assays, cells were treated with 100 μg/ml cycloheximide (Santa Cruz Biotechnology) for the indicated time points. After treatment, cells were resuspended in SDS-PAGE sample buffer and boiled for 10 min at 95 °C before SDS-PAGE and western blot analysis.

RNA extraction and qRT-PCR

RNA was purified using TriPure Isolation Reagent (Sigma-Aldrich) according to the manufacturer's instructions. For cDNA synthesis, 1 μg of RNA was retro-transcribed with MMLV-RT (ThermoFisher Scientific) and random hexamers (ThermoFisher Scientific) according to the manufacturer's instructions. qPCR were performed using KAPA SYBR FAST (Sigma-Aldrich) and primers described in the Supplemental Table 1.

qTRAP

Telomerase activity was measured in cell extracts as described previously (Viceconte et al., 2017). About 2 million of cells were resuspended into 200 μl of Lysis CHAPS buffer (1 mM MgCl2, 1 mM EGTA, 10 mM Tris-HCl pH 7.5, 10% v/v glycerol, 5 mg/ml CHAPS) containing 1 μl/ml β-mercaptoethanol and Complete Mini protease inhibitors (see Key Resources Table). After incubation for 30 min at 4°C under rotation, samples were centrifuged for 5 min at 12 000 rpm at 4°C in an Eppendorf centrifuge. Protein concentration was measured in the supernatant and 100 ng of protein extracts

were mixed with 0.5 μl primer TS 10 μM, 0.5 μl primer ACX 10 μM and 10 μl KAPA SYBR FAST (Supplemental Table 1 and Key Resources Table) in a final volume of 20 μl. Samples were then incubated in a thermocycler using the following program: 25°C for 30 min, 95°C for 5 min, 40 cycles with 95°C for 30 sec, 60°C for 30 sec and 72°C for 90 sec and, finally, 95°C for 30 sec.

Telomere restriction fragment (TRF) analysis

TRF analysis was performed by Southern blot using a radioactive $(CCCTAA)_4$ probe as described previously (Viceconte et al., 2017). After overnight digestion of 10 μg RNAse-treated genomic DNA with 20 U *Hinf*I and 20 U *Rsa*I, samples were loaded on a 0.8% agarose gel in TAE 1x buffer and migration was performed for 6 h at 75 V. DIG markers from the Telo*TAGGG* kit (Key Resources Table) were included. Gel treatment, capillary transfer and pre-hybridization were performed according to the Telo*TAGGG* kit's instructions. Hybridization of the membrane was performed by incubation for 16 h at 42°C in 12 ml DIG Easy Hyb solution (provided in the Telo*TAGGG* kit) containing the radioactive telomere probe prepared as follows: the telomeric probe $(CCCTAA)_4$ (10 μM) was denatured for 5 min at 68°C. One μl of the probe was then radioactively labeled with 6 μl of [γ-^{32}P]ATP (10 mCi/ml) (Perkin-Elmer) and 1 μl of T4 poly-nucleotide kinase (Sigma-Aldrich) (10 U/μl) in a total volume of 20 μl of 1x PNK buffer. This mix was incubated for 20 min at 37°C and T4 PNK was then inactivated by the addition of 2 μl of EDTA (0.5M, pH 8.0). Forty μl of 1x PNK buffer were then added to the radioactive probe before purification on a G-25 column.

After hybridization, the medium was discarded and the membrane was washed first with Stringent wash buffer I for 20 min at RT and then with pre-warmed Stringent wash buffer II for 10 min at 50°C (buffers provided in the Telo*TAGGG* kit). The membrane was then exposed to an X-ray film before revelation.

Methylation-Specific (MS) PCR

Genomic DNA was isolated from cells by phenol-chloroform extraction and isopropanol precipitation methods. For bisulfite treatment of DNA and MS-PCR, we adapted the procedure described by Jung et al. (2008). Two μg of genomic DNA were denatured by NaOH (0.375M) in a volume of 40 μl for 10 min at RT. To this mix, 260 μl of a freshly prepared solution of 4.5 M sodium bisulfite (Acros Organics) and 0.5 mM

hydroquinone (Chimica) pH 5.0 were added and mixed and samples were incubated overnight at 50°C with 5 min at 95°C every 3 hours. DNA was purified using GENECLEAN® kit (MP Biomedicals) following the manufacturer's instructions and eluted in 50 µl of water. Modification was completed by a 10 min incubation with 0.3M NaOH at room temperature. The DNA was then precipitated and resuspended in 40 µl. Primer sequences for MSP of the TSPYL5 are listed in the Supplemental Table 1. PCR amplification was performed with KAPA SYBR® FAST DNA Polymerase (Key Resources Table) under the following conditions: 95°C for 10 min, then 40 cycles of 95°C for 15 s and 60°C for 30 s. The amplified PCR products were separated on a 1.5% agarose gel.

Immunofluorescence and DNA-FISH

Immunofluorescence was performed as described previously (Boros et al., 2014) using antibodies listed in the Key Resources Table. TIF detection was performed as described previously (Diman et al., 2016) using TeloG Exiqon LNA™red probe (TAMRA) GGGTtAGGGttAGgGTTAGGGttAGGGttAGGGtTA(TAMRA) (small letters indicate LNA™ modified bases). The day before the experiment, cells were seeded on 4-well slides (20 000 cells/well with 150 µl medium). The next day, cells were washed twice with PBS 1x before incubation for 5 min at room temperature (RT) with Permeabilization buffer (20 mM Tris-HCl pH 8.0, 50 mM NaCl, 3 mM $MgCl_2$, 300 mM sucrose, 0.5% Triton X-100). Then, cells were fixed with 3% formaldehyde and 2% sucrose in PBS 1x for 15 min at RT. After 3 washes of 3 min each with PBS 1x at RT, cells were again incubated with Permeabilization buffer for 10 min at RT. Cells were then washed 3 times for 3 min with PBS 1x before incubation for 1 h at 37°C with 150 µl/well of Blocking solution (10% normal goat serum (Cell Signaling Technology), 1% BSA, 0.1% Triton X-100 in PBS 1x). Add the primary antibody in the Blocking solution and incubate ON at 4°C (TRF2: 1/500; TSPYL5: 1/50; POT1: 1/100; TPP1: 1/250; 53BP1: 1/600; PML(ab53773): 1/150, PML(sc-966): 1/100, HA: 1/50, USP7: 1/1000; ATRX: 1/300). Cells were then washed 3 times for 3 min with 0.1% Tween-20 in PBS 1x at 45°C. If relevant, cells were incubated with a second primary antibody diluted into 40 µl of Blocking solution for 45 min at 37°C. After 3 washes for 3 min each with 0.1% Tween-20 in PBS 1x at 45°C, cells were incubated with the secondary antibody diluted

(1:400) into 100-150 μl Blocking solution for 40 min at 37°C. Cells were again washed 3 times for 3 min each with 0.1% Tween-20 in PBS 1x at 45°C before a last series of 3 washes for 3 min each with PBS 1x at RT. In the absence of FISH, cells were air dried and mounted with 20-25 μl/well of mounting medium (23.5 mg/ml DABCO (Sigma-Aldrich), 20 mM Tris-HCl pH 7.4, 90% v/v glycerol) containing 0.6 μg/ml DAPI.

If FISH was performed after IF, cells were fixed again for 2 min with 3.7% formaldehyde in PBS 1x. After 3 washes for 3 min each with PBS 1x at RT, cells were incubated with 150 μl RNAse A solution (0.1 mg/ml) for 1 h at RT. Cells were then washed 3 times for 3 min with SSC 2x before incubation for 10 min at RT with the Permeabilization buffer. After a brief wash with PBS 1x, cells were fixed again for 2 min with 3.7% formaldehyde in PBS 1x and washed 3 times for 3 min with PBS 1x. Dehydration of the cells was next performed by successive incubations of 2 min each in 70%, 80%, 90% and 100% ethanol. Slides were air dried. For hybridization with the LNA probe, cells were overlaid with 35 μl of Hybridization solution (160 nM G-rich red LNA telomeric probe (see Supplemental Table 1), 50% deionized formamide, SSC 2x, Blocking reagent 1x (Sigma-Aldrich)) and incubated at 83°C for 3 min with a coverslip. Then, a second incubation of 2 h at RT was performed before successive washes as follows: 2x15 min in 50% formamide, SSC 2x, 20 mM Tris-HCl pH 7.4 and 3x5 min in 150 mM NaCl, 0.05% Tween-20, 50 mM Tris-HCl pH 7.4. Dehydration of the cells was performed as described above, slides were air dried and mounted with 20-25 μl/well of mounting medium (23.5 mg/ml DABCO (Sigma-Aldrich), 20 mM Tris-HCl pH 7.4, 90% v/v glycerol) containing 0.6 μg/ml DAPI.

Images were acquired with the Cell Observer Spinning Disk confocal microscope (Zeiss) with 100X objective and analyzed using ImageJ software (National Institute of Health). All experiments were repeated at least 2 times (in most cases 3 times) and representative pictures are shown in the figures.

Western blotting

Total cell extracts were prepared with RIPA buffer (150 mM NaCl, 50 mM Tris-HCl pH 8.0, 1% NP-40, 0.5% Sodium Deoxycholate, 0.1% SDS, 1 mM EDTA). Western blotting was performed according to standard procedures using antibodies described in the Key Resources Table. Revelation was performed with SuperSignal West Pico

Chemiluminescent Substrate (ThermoFisher Scientific). Signal quantification was done using ImageJ software (National Institute of Health). All experiments were repeated at least 2 times and representative blots are shown in the figures.

Immunoprecipitation experiments

Cells were lysed with NP-40 lysis buffer (50 mM Tris-HCl pH 8, 5 mM EDTA, 150 mM NaCl, 1% NP-40) supplemented with protease inhibitors (Complete Mini, Sigma-Aldrich). After lysis, 500 μg of proteins were incubated overnight with 5 μg of primary antibody (listed in the Key Resources Table) or irrelevant IgG. Protein complexes were immunoprecipitated with protein G agarose beads (ThermoFisher Scientific) for 30 min at 4°C and 30 min at room temperature. Beads were then washed 2 times with NP-40 lysis buffer. Bound proteins were eluted with SDS-PAGE sample buffer, boiled for 10 min at 95 °C and analyzed by western blot.

Detection of POT1 and TPP1 ubiquitination

For detection of POT1poly- ubiquitination, U2OS/ALT$^+$ cells were transfected with pLPC-myc-hPOT1 and HA-Ubiquitin plasmids (Key Resources Table). After 42 hours, cells were incubated with 10 μM MG132 (Sigma-Aldrich) for 6 hours, before lysis with NP-40 buffer and immunoprecipitation with 5 μg anti-Myc antibody as described above. For detection of TPP1 ubiquitination, we followed the protocol described by Zemp and Lingner (2014). 48 h after transfection of U2OS/ALT$^+$ cells with pCI-His-hUbi and pCDNA-3xFLAG-NLS-TPP1 plasmids (Key Resources Table), cells were treated with 10 μM MG132 (Sigma-Aldrich) for 2 hours and harvested into cold PBS containing 0.5 mM EDTA and 2 mM N-ethylmaleimide. After centrifugation at 400 x *g* for 4 min at 4°C, cells were resuspended into 300 μl of urea lysis buffer (8 M urea, 100 mM sodium phosphate, pH 8.0, 15 mM imidazole). After sonication (25 pulses), cell lysates were incubated for 10 min at RT on a rotating wheel before centrifugation at RT for 10 min at 20,000 x *g*. 20 μl of Ni-NTA agarose beads (Key Resources Table) were incubated with 2-4 mg of total protein extracts during 4 h at RT on a rotating wheel. After incubation, beads were washed twice with 800 μl of 6 M guanidine-HCl, 100 mM sodium phosphate, pH 8.0, 0.5% Triton X-100 and 15 mM imidazole and once with 800 μl of urea lysis buffer. Bound proteins were eluted with 25 μl of urea lysis buffer containing

100 mM imidazole by incubation for 5 min at RT. SDS-PAGE loading buffer was directly added to the eluate.

All experiments were repeated at least 2 times and representative blots are shown in the figures.

Cell fractionation

Cell fractionation was performed using the protocol previously described by Méndez and Stillman (2000). Trypsinized cells were resuspended in medium containing serum, collected by centrifugation, and washed with ice-cold PBS. All procedures were performed on ice. Cells were resuspended into ice-cold Solution A (10 mM HEPES, pH 7.9, 10 mM KCl, 1.5 mM $MgCl_2$, 0.34 M sucrose (Sigma-Aldrich), 10% glycerol, 1 mM dithiothreitol (Millipore), 1 mM phenylmethylsulfonyl fluoride (Sigma-Aldrich), and 1x Complete Mini protease inhibitors (Sigma-Aldrich). Triton X-100 (0.1%) (Sigma-Aldrich) was added, and the cells were incubated for 10 min at 4°C on a rotating wheel. Nuclei were collected in the pellet by low-speed centrifugation (4 min, 1,300 x*g*, 4°C). The supernatant was collected as the cytoplasm fraction and further clarified by high-speed centrifugation (15 min, 20,000g, 4°C) to remove cell debris and insoluble aggregates. Nuclei were washed once in Solution A and then lysed in Solution B (3 mM EDTA, pH 8.0, 0.2 mM EGTA, 1 mM DTT, 1x Complete Mini protease inhibitors (Sigma-Aldrich)) by incubation for 30 min at 4˚C on a rotating wheel. The lysate was further fractionated into nucleoplasm (supernatant) and chromatin (pellet) fraction by centrifugation at 1,700g for 4 min at 4°C. The pellet was resuspended into Laemmli sample buffer and boiled at 98°C for 5 min before sonication.

Cellular viability measurement

For cell viability measurements, the WST-1 reagent (Sigma-Aldrich, see Key Resources Table) was used. Three days after the first siRNA transfection, cells were re-transfected and seeded into 96-well plates. After another 72 h, cells were incubated for 3 h in 100 µl of medium containing 10 µl of WST-1 reagent, according to the manufacturer's instructions. After incubation, the absorbance was measured at 450 nm using a plate reader. All experiments were repeated at least 3 times.

Annexin V-FITC flow cytometric analysis

Cell death was evaluated using the FITC Annexin V Apoptosis Detection Kit II (BD Biosciences) following the manufacturer's instructions. Fluorescent activated cell sorting was performed using a BD FACSVerse™ flow cytometer, and at least 10,000 events were recorded and represented as dot plots. FlowJo software was used for data analysis. Positive controls for apoptosis were obtained by treating cells with 50 μM etoposide (Sigma-Aldrich) for 24 hours. All experiments were repeated 3 times.

Quantification and Statistical Analysis

ImageJ was used for quantification of western blots and analysis of confocal microscopy pictures. Microsoft Excel was used for Student's *t*-tests to compare differences between means.

Data and Software Availability

Unprocessed imaging data are deposited on Mendeley Data: http://dx.doi.org/10.17632/nvbwtcmdwk.1

KEY RESOURCES TABLE

REAGENT or RESOURCE	SOURCE	IDENTIFIER
Antibodies		
Anti-β-actin (WB)	Sigma-Aldrich	Cat #A5441; RRID:AB_476744
Anti-TSPYL5 (WB and IF)	Santa Cruz	Cat #sc-98186; RRID:AB_2211377
Anti-POT1 (WB and IF)	Abcam	Cat #ab124784; RRID:AB_10975313
Anti-TPP1 (WB and IF)	Bethyl	Cat #A303-069A; RRID:AB_10890369
Anti-ATRX (IF)	Sigma-Aldrich	Cat #HPA001906; RRID:AB_1078249
Anti-TRF2 (WB)	Novus Biologicals	Cat #NB110-57130; RRID:AB_844199
Anti-TRF2 (IF)	IMGENEX	Cat #IMG-124A; RRID:AB_317546
Anti-TRF1 (WB)	Abcam	Cat #ab129177; RRID:AB_11142009
Anti-RAP1 (WB)	Bethyl	Cat #A300-306A; RRID:AB_162721
Anti-H3 (WB)	Abcam	Cat #ab1791; RRID:AB_302613

Anti-GAPDH (WB)	Millipore	Cat #MAB374; RRID:AB_2107445
Anti-USP7 (WB)	Abcam	Cat #ab190183; RRID:AB_2752248
Anti-HA (WB and IF)	Sigma-Aldrich	Cat #H6908; RRID:AB_260070
Anti-FLAG (IP)	Sigma-Aldrich	Cat #F1084; RRID:AB_2752249
Anti-MYC (IP)	Cell Signaling Technology	Cat #2276; RRID:AB_331783
Anti-PML (IF)	Abcam	Cat #ab53773; RRID:AB_882092
Anti-PML (IF)	Santa Cruz	Cat #sc-966; RRID:AB_628162
Anti-53BP1 (IF)	Novus Biologicals	Cat #NB100-304; RRID:AB_10003037
HRP-Anti-rabbit IgG (WB)	Enzo Life Sciences	Cat #ADI-SAB-300-J; RRID:AB_11179983
HRP-Anti-mouse IgG (WB)	Santa Cruz	Cat #sc-2005; RRID:AB_631736
Alexa 488-Anti-rabbit IgG (IF)	ThermoFisher Scientific	Cat #A-11008; RRID:AB_143165
Alexa 546-Anti-mouse IgG (IF)	ThermoFisher Scientific	Cat #A-11003; RRID:AB_141370
Alexa 546-Anti-rabbit IgG (IF)	ThermoFisher Scientific	Cat #A-11010; RRID:AB_143156
Alexa 488-Anti-mouse IgG (IF)	ThermoFisher Scientific	Cat #A-11001; RRID:AB_2534069
Alexa 647-Anti-mouse IgG (IF)	ThermoFisher Scientific	Cat #A-31571; RRID:AB_162542
Bacterial and Virus Strains		
DH5α	ThermoFisher Scientific	Cat #18265017
Chemicals, Peptides, and Recombinant Proteins		
MG132 proteasome inhibitor	Sigma-Aldrich	Cat #474790
Cycloheximide	Santa Cruz Biotechnology	Cat #sc-3508
Complete Mini protease inhibitors	Sigma-Aldrich	Cat #11836153001
Hygromycin B	Sigma-Aldrich	Cat #H3274
Geneticin (G418)	MP Biomedicals	Cat #091672546
Lipofectamine 2000	ThermoFisher Scientific	Cat #11668019
Polyethylenimine, linear, MW 25000 (PEI 25K)	Polysciences, Inc.	Cat #23966-1
TriPure Isolation Reagent	Sigma-Aldrich	Cat #11667165001
M-MLV reverse transcriptase	ThermoFisher Scientific	Cat #28025-013
Critical Commercial Assays		
GeneChIP® WT PLUS Reagent kit	ThermoFisher Scientific	Cat #902280
GeneChIP® Human Transcriptome Array 2.0	ThermoFisher Scientific	Cat #902162
Cell Proliferation Reagent WST-1	Sigma-Aldrich	Cat #5015944001

FITC Annexin V Apoptosis Detection Kit II	BD Biosciences	Cat #556570
KAPA SYBR FAST	Sigma-Aldrich	Cat #KK4602
SuperSignal West Pico Chemiluminescent Substrate	ThermoFisher Scientific	Cat #34580
Telo*TAGGG* Telomere Length Assay	Sigma-Aldrich	Cat #12209136001
Deposited Data		
Unprocessed imaging data (Mendeley Data)	This paper	http://dx.doi.org/10.17632/nvbwtcmdwk.1
Experimental Models: Cell Lines		
Human: SW39/TEL$^+$ (SV40T immortalized IMR90 fetal lung fibroblasts)	Kindly provided by W. Wright, UT Southwestern, Dallas, USA	N/A
Human: IMRB/ALT$^+$ (SV40T immortalized IMR90 fetal lung fibroblasts)	Coriell Institute for Medical Research	AG03204
Human: SI14/TEL$^+$ (1st hybridization)	Episkopou *et al*., 2014	N/A
Human: SI27/TEL$^+$ (1st hybridization)	Episkopou *et al*., 2014	N/A
Human: 6C3/TEL$^+$ (2nd hybridization)	This paper	N/A
Human: SI24/ALT$^+$ (1st hybridization)	Episkopou *et al*., 2014	N/A
Human: 8G12/ALT$^+$ (2nd hybridization)	This paper	N/A
Human: 7F10/ALT$^+$ (2nd hybridization)	This paper	N/A
Human: VA13/ALT$^+$ (SV40T immortalized WI38 fetal lung fibroblasts-subline 2RA)	Kindly provided by J.A. Londoño-Vallejo, Curie Institute, Paris, France	ATCC CCL-75.1
Human: HFF2 (primary foreskin fibroblasts)	ATCC	ATCC SCRC-1042
Human: U2OS/ALT$^+$ (osteosarcoma)	Kindly provided by F. Fuks, F. Journe and H.I. Boufker ULB, Brussels, Belgium	ATCC HTB-96
Human: SaOS-2/ALT$^+$ (osteosarcoma)	Kindly provided by F. Fuks, F. Journe and H.I. Boufker ULB, Brussels, Belgium	ATCC HTB-85
Human: MG63/TEL$^+$ (osteosarcoma)	Kindly provided by F. Fuks, F. Journe and H.I. Boufker ULB, Brussels, Belgium	ATCC CRL-1427
Human: HT1080/TEL$^+$ (fibrosarcoma)	Kindly provided by J. Lingner, EPFL, Lausanne, Switzerland	ATCC CCL-121
Human: 143B/TEL$^+$ (osteosarcoma)	Coriell Institute for Medical Research	GM05887
Oligonucleotides		
See Table S1		
Recombinant DNA		
Plasmid: pLPC-myc-hPOT1	Loayza and de Lange, 2003	Addgene Plasmid #12387
Plasmid: pLPC-myc	Kind gift from T. de Lange	Addgene Plasmid #12540

Plasmid: pCDNA-3xFLAG-NLS-TPP1	Zhong *et al.,* 2012	Addgene Plasmid #53585
Plasmid: HA-Ubiquitin	Kamitani *et al*., 1997	Addgene Plasmid #18712
Plasmid: pCI-His-hUbi	Young *et al*., 2011	Addgene Plasmid #31815
Plasmid: pcDNA6-3xHA-TPP1 (WT)	Kind gift from J. Lingner (EPFL, Lausanne, Switzerland); Zemp and Lingner, 2014	N/A
Plasmid: pcDNA6-3xHA-TPP1 (10R)	Kind gift from J. Lingner (EPFL, Lausanne, Switzerland); Zemp and Lingner, 2014	N/A
Plasmid: pcDNA6-3xHA-TPP1 (S132A)	Kind gift from J. Lingner (EPFL, Lausanne, Switzerland); Zemp and Lingner, 2014	N/A
Software and Algorithms		
ImageJ	National Institute of Health	N/A
Other		
Protein G agarose beads	Thermo Fisher Scientific	Cat #20398
Ni-NTA agarose beads	Thermo Fisher Scientific	Cat #60-0441
Normal goat serum	Cell Signaling Technology	Cat #5425S

Supplementary Excel Table Legends

Table S1. Oligonucleotides used in this study. Related to STAR Methods.

References

An, L., Jiang, Y., Ng, H.H.W., Man, E.P.S., Chen, J., Khoo, U.-S., Gong, Q., and Huen, M.S.Y. (2017). Dual-utility NLS drives RNF169-dependent DNA damage response. Proc. Natl. Acad. Sci. USA. *114*, E2872-E2881.

Arnoult, N., Van Beneden, A., and Decottignies, A. (2012). Telomere length regulates TERRA levels through increased trimethylation of telomeric H3K9 and HP1α. Nat. Struct. Mol. Biol. *19*, 948-956.

Baerlocher, G.M. et al. (2015). Telomerase inhibitor imetelstat in patients with essential thrombocythemia. N. Engl. J. Med. *373*, 920-928.

Boros, J., Arnoult, N., Stroobant, V., Collet, J.-F., and Decottignies, A. (2014). Polycomb repressive complex 2 and H3K27me3 cooperate with H3K9 methylation to maintain heterochromatin protein 1α at chromatin. Mol. Cell. Biol. *34*, 3662-3674.

Bower, K., Napier, C.E., Cole, S.L., Dagg, R.A., Lau, L.M., Duncan, E.L., Moy, E.L., and Reddel, R.R. (2012). Loss of wild-type ATRX expression in somatic cell hybrids segregates with activation of Alternative Lengthening of Telomeres. PLoS One *7*, e50062.

Canning, M., Boutell, C., Parkinson, J., and Everett, R.D. (2004). A RING finger ubiquitin ligase is protected from autocatalyzed ubiquitination and degradation by binding to ubiquitin-specific protease USP7. J. Biol. Chem. *279*, 38160-38168.

Cao, T., Duprez, E., Borden, K.L., Freemont, P.S., and Etkin, L.D. (1998). Ret finger protein is a normal component of PML nuclear bodies and interacts directly with PML. J. Cell Sci. *111*, 1319-1329.

Cesare, A.J., and Reddel, R.R. (2010). Alternative lengthening of telomeres: models, mechanisms and implications. Nat. Rev. Genet. *11*, 319-330.

Chen, L.Y., Liu, D., and Songyang, Z. (2007). Telomere maintenance through spatial control of telomeric proteins. Mol. Cell. Biol. *27*, 5898-5909.

Chen, C. et al. (2017). Structural insights into POT1-TPP1 interaction and POT1 C-terminal mutations in human cancer. Nat. Comm. *8*, 14929.

Cheng, X., and Kao, H.-Y. (2013). Post-translational modifications of PML: consequences and implications. Front. Oncol. *2*, 210.

Dagg, R.A. et al. (2017). Extensive proliferation of human cancer cells with ever-shorter telomeres. Cell Rep. *19*, 2544-2556.

de Lange, T. (2005). Shelterin: the protein complex that shapes and safeguards human telomeres. Genes Dev. *19*, 2100-2110.

Déjardin, J., and Kingston, R.E. (2009). Purification of proteins associated with specific genomic loci. Cell *136*, 175-186.

Denchi, E.L., and de Lange, T. (2007). Protection of telomeres through independent control of ATM and ATR by TRF2 and POT1. Nature *448*, 1068-1071.

Diman, A., Boros, J., Poulain, F., Rodriguez, J., Purnelle, M., Episkopou, H., Bertrand, L. Francaux, M., Deldicque, L., and Decottignies, A. (2016). Nuclear respiratory factor 1 and endurance exercise promote human telomere transcription. Sci. Adv. *2*: e1600031.

Draskovic, I., Arnoult, N., Steiner, V., Bacchetti, S., Lomonte, P., and Londoño-Vallejo, A. (2009). Probing PML body function in ALT cells reveals spatiotemporal requirements for telomere recombination. Proc. Natl. Acad. Sci. USA *106*, 15726-15731.

Episkopou, H., Draskovic, I., Van Beneden, A., Tilman, G., Mattiussi, M., Gobin, M., Arnoult, N., Londoño-Vallejo, A., and Decottignies, A. (2014). Alternative lengthening

of telomeres is characterized by reduced compaction of telomeric chromatin. Nucleic Acids Res. *42*, 4391-4405.

Epping, M.T., Meijer, L.A., Krijgsman, O., Bos, J.L., Pandolfi, P.P., and Bernards, R. (2011). TSPYL5 suppresses p53 levels and function by physical interaction with USP7. Nat. Cell Biol. *13*, 102-108.

Escoffier, E., Rezza, A., Roborel de Climens, A., Belleville, A., Gazzolo, L., Gilson, E., and Duc Dodon, M. (2005). A balanced transcription between telomerase and the telomeric DNA-binding proteins TRF1, TRF2 and Pot1 in resting, activated, HTLV-1-transformed and Tax-expressing human T lymphocytes. Retrovirology *2*, 77.

Everett, R.D., Rechter, S., Papior, P., Tavalai, N., Stamminger, T., and Orr, A. (2006). PML contributes to a cellular mechanism of repression of herpes simplex virus type 1 infection that is inactivated by ICP0. J. Virol. *80*, 7995-8005.

Frink, R.E., Peyton, M., Schiller, J.H., Gazdar, A.F., Shay, J.W., and Minna, J.D. (2016). Telomerase inhibitor imetelstat has preclinical activity across the spectrum of non-small cell lung cancer oncogenotypes in a telomere length dependent manner. Oncotarget *7*, 31639-31651.

Gallagher, W.M. et al. (2005). Multiple markers for melanoma progression regulated by DNA methylation: insights from transcriptomic studies. Carcinogenesis. *26*, 1856-1867.

Garcia-Exposito, L. et al. (2016). Proteomic profiling reveals a specific role for translesion DNA polymerase η in the alternative lengthening of telomeres. Cell Rep. *17*, 1858-1871.

Gong, Y., and de Lange, T. (2010). A Shld1-controlled POT1a provides support for repression of ATR signaling at telomeres through RPA exclusion. Mol. Cell *40*, 377-387.

Iconomou, M., and Saunders, D.N. (2016). Systematic approaches to identify E3 ligase substrates. Biochem. J. *473*, 4083-4101.

Jung, Y., Park, J., Bang, Y.J., and Kim, T.Y. (2008). Gene silencing of TSPYL5 mediated by aberrant promoter methylation in gastric cancers. Lab. Invest. *88*, 153-160.

Kamitani, T., Kito, K., Nguyen, H.P., and Yeh, E.T. (1997). Characterization of NEDD8, a developmentally down-regulated ubiquitin-like protein. J. Biol. Chem. *272*, 28557-28562.

Karlseder, J., Broccoli, D., Dai, Y., Hardy, S., and de Lange, T. (1999). p53- and ATM-dependent apoptosis induced by telomeres lacking TRF2. Science *283*, 1321-1325.

Kim, R.Q., and Sixma, T.K. (2017). Regulation of USP7: a high incidence of E3 complexes. J. Mol. Biol. *429*, 3395-3408.

Kondo, T., Oue, N., Yoshida, K., Mitani, Y., Naka, K., Nakayama, H., and Yasui, W. (2004). Expression of POT1 is associated with tumor stage and telomere length in gastric carcinoma. Cancer Res. *64*, 523-529.

Li, M., Brooks, C.L., W. Gu, W. (2004). A dynamic role of HAUSP in the p53-Mdm2 pathway. Mol. Cell *13***,** 879-886.

Liu, D., Safari, A., O'Connor, M.S., Chan, D.W., Laegeler, A., Qin, J., and Songyang, Z. (2004). PTOP interacts with POT1 and regulates its localization to telomeres. Nat. Cell Biol. *6*, 673-680.

Loayza, D., and de Lange, T. (2003). POT1 as a terminal transducer of TRF1 telomere length control. Nature *423*, 1013-1018.

Méndez, J., and Stillman, B. (2000). Chromatin association of human origin recognition complex, Cdc6, and mibichromosome maintenance proteins during the cell cycle: assembly of prereplication complexes in late mitosis. Mol. Cell. Biol. *20*, 8602-8612.

Nicklas, S., Hillje, A.L., Okawa, S., Rudolph, I.M., Collmann, F.M., van Wuellen, T., Del Sol, A., and Schwamborn, J.C. (2019). A complex of the ubiquitin ligase TRIM32 and the deubiquitinase USP7 balances the level of c-Myc ubiquitination and thereby determines neural stem cell fate specification. Cell Death Differ. *26*, 728-740.

Osterwald, S., Deeg, K.I., Chung, I., Parisotto, D., Wörz, S., Rohr, K., Erfle, H., and Rippe, K. (2015). PML induces compaction, TRF2 depletion and DNA damage signaling at telomeres and promotes their alternative lengthening. J. Cell Sci. *128*, 1887-1890.

Pickett, H.A., and Reddel, R.R. (2015). Molecular mechanisms of activity and derepression of alternative lengthening of telomeres. Nat. Struct. Mol. Biol. *22*, 875-880.

Poncet, D. et al. (2008). Changes in the expression of telomere maintenance genes suggest global telomere dysfunction in B-chronic lymphocytic leukemia. Blood *111*, 2388-2391.

Potts, P.R., and Yu, H. (2007). The SMC5/6 complex maintains telomere length in ALT cells through SUMOylation of telomere-binding proteins. Nat. Struct. Mol. Biol. *14*, 581-590.

Rai, R., Li, J.M., Zheng, H., Lok, G.T., Deng, Y., Huen, M.S., Chen, J., Jin, J., and Chang, S. (2011). The E3 ubiquitin ligase Rnf8 stabilizes Tpp1 to promote telomere end protection. Nat. Struct. Mol. Biol. *18*, 1400-1407.

Rockel, T.D., Stuhlmann, D., and von Mikecz, A. (2005). Proteasomes degrade proteins in focal subdomains of the human cell nucleus. J. Cell Sci. *118*, 5231-5242.

Salomoni, P. (2013). The PML-interacting protein DAXX: histone loading gets into the picture. Front. Oncol. *3*, 152.

Sarkari, F., Wang, X., Nguyen, T., and Frappier, L. (2011). The Herpesvirus associated ubiquitin specific protease, USP7, is a negative regulator of PML proteins and PML nuclear bodies. PLoS One *6*, e16598.

Tang, J., Qu, L.K., Zhang, J., Wang, W., Michaelson, J.S., Degenhardt, Y.Y., El-Deiry, W.S., and Yang, X. (2006). Critical role for Daxx in regulating Mdm2. Nat. Cell Biol. *8*, 855-862.

Tefferi, A. et al. (2015). A pilot study of the telomerase inhibitor imetelstat for myelofibrosis. N. Engl. J. Med. *373*, 908-919.

Tilman, G., Loriot, A., Van Beneden, A., Arnoult, N., Londoño-Vallejo, J. A., De Smet, C., and Decottignies, A. (2009). Subtelomeric DNA hypomethylation is not required for telomeric sister chromatid exchanges in ALT cells. Oncogene *28*, 1682-1693.

Viceconte, N., Dheur, M.-S., Majerova, E., Pierreux, C.E., Baurain, J.-F., van Baren, N., and Decottignies, A. (2017). Highly aggressive metastatic melanoma cells unable to maintain telomere length. Cell Rep. *19*, 2529-2543.

Vogel, T., Dittrich, O., Mehraein, Y., Dechend, F., Schnieders, F. and Schmidtke, J. (1998). Murine and human TSPYL genes: novel members of the TSPY-SET-NAP1L1 family. Cytogenet Cell Genet. *81*, 265-270.

Wang, F., Podell, E.R., Zaug, A.J., Yang, Y., Baciu, P., Cech, T.R., and Lei, M. (2007). The POT1-TPP1 telomere complex is a telomerase processivity factor. Nature *445*, 506-510.

Wei, X., Yu, Z.K., Ramalingam, A., Grossman, S.R., Yu, J.H., Bloch, D.B., and Maki, C.G. (2003). Physical and functional interactions between PML and MDM2. J. Biol. Chem. *278*, 29288-29297.

Ye, J.Z., Hockemeyer, D., Krutchinsky, A.N., Loayza, D., Hooper, S.M., Chait, B.T., and de Lange, T. (2004). POT1-interacting protein PIP1: a telomere length regulator that recruits POT1 to the TIN2/TRF1 complex. Genes Dev. *18*, 1649-1654.

Young, J.A., Sermwittayawong, D., Kim, H.J., Nandu S., An, N., Erdjument-Bromage, H., Tempst, P., Coscoy, L., and Winoto, A. (2011). Fas-associated death domain (FADD) and the E3 ubiquitin-protein ligase TRIM21 interact to negatively regulate virus-induced interferon production. J. Biol. Chem. *286*, 6521-6531.

Zemp, I., and Lingner, J. (2014). The shelterin component TPP1 is a binding partner and substrate for the deubiquitinating enzyme USP7. J. Biol. Chem. *289*, 28595-28606.

Zhong, F.L., Batista, L.F., Freund, A., Pech, M.F., Venteicher, A.S., and Artandi, S.E. (2012). TPP1 OB-fold domain controls telomere maintenance by recruiting telomerase to chromosome ends. Cell *150*, 481-494.

Figure 1

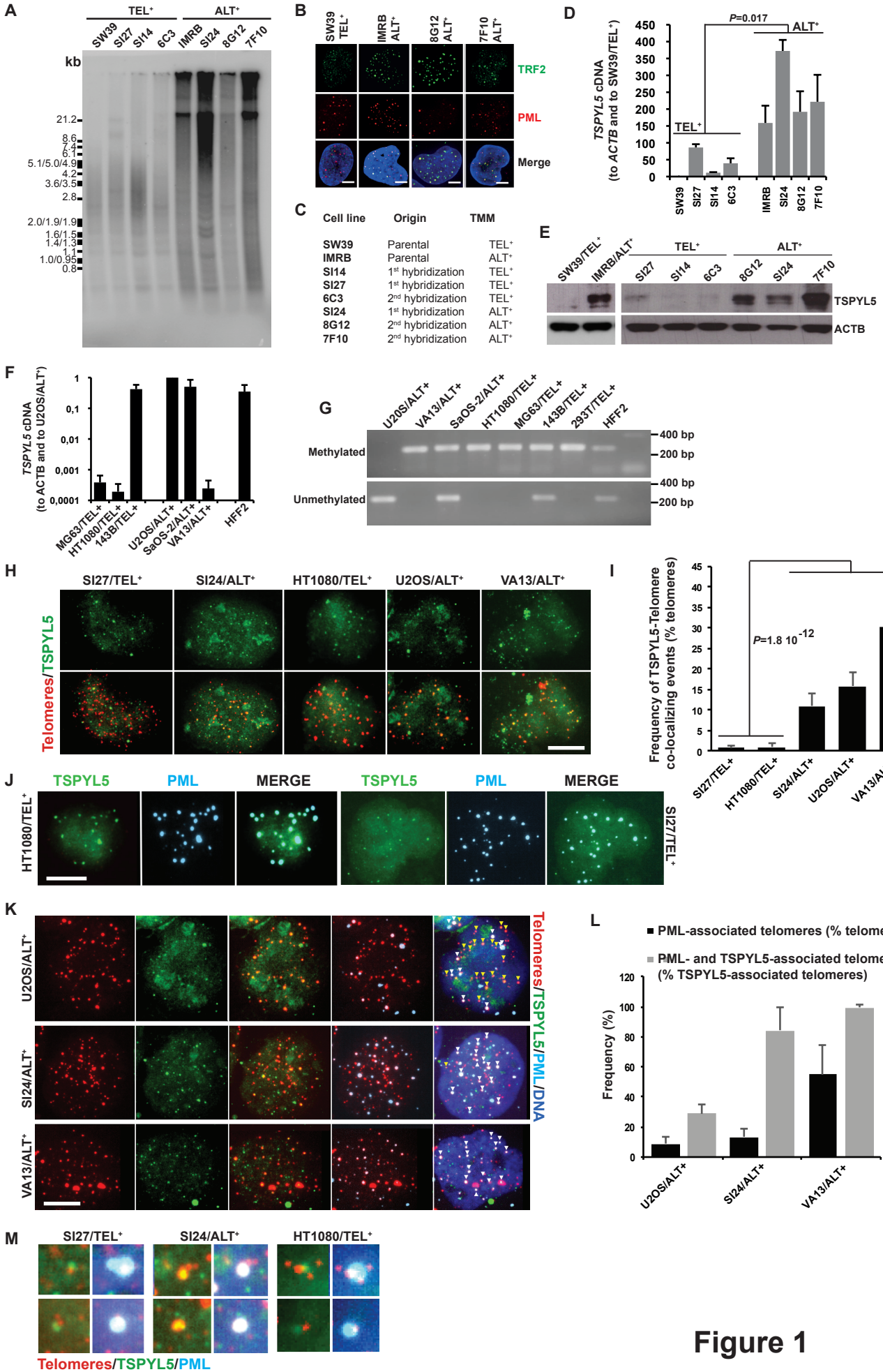

Figure 1

Figure 2

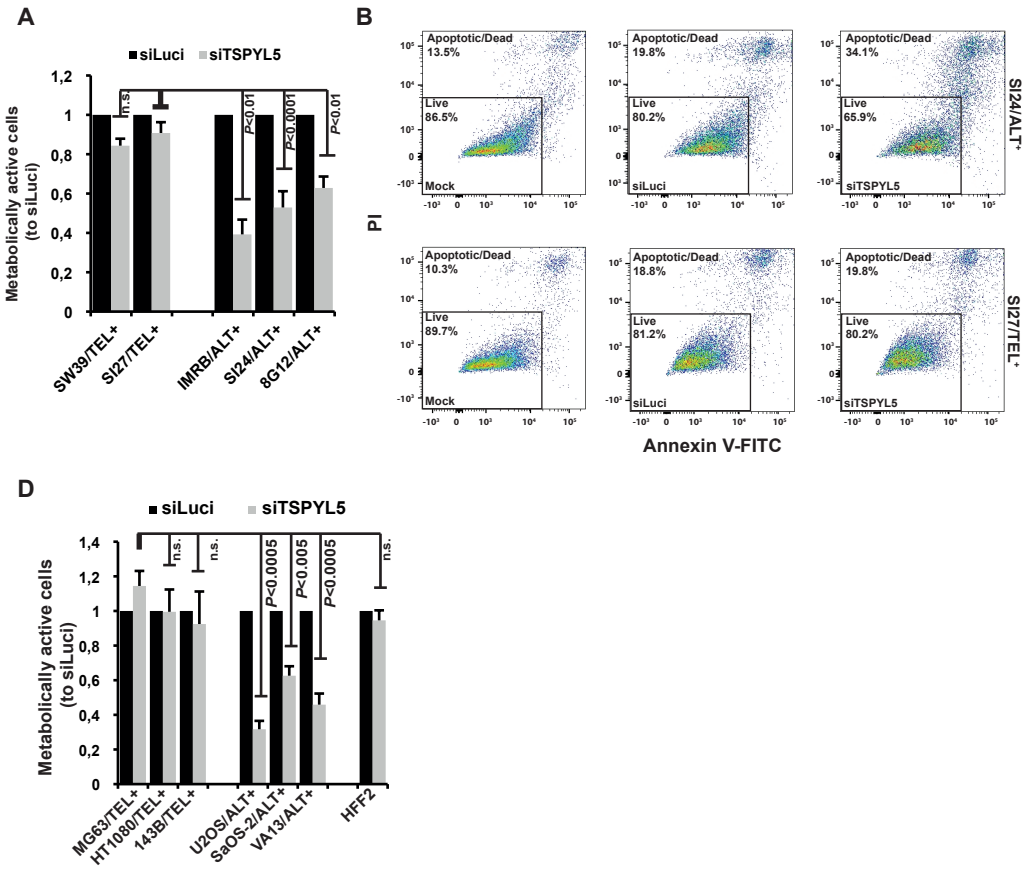

Figure 2

Figure 3

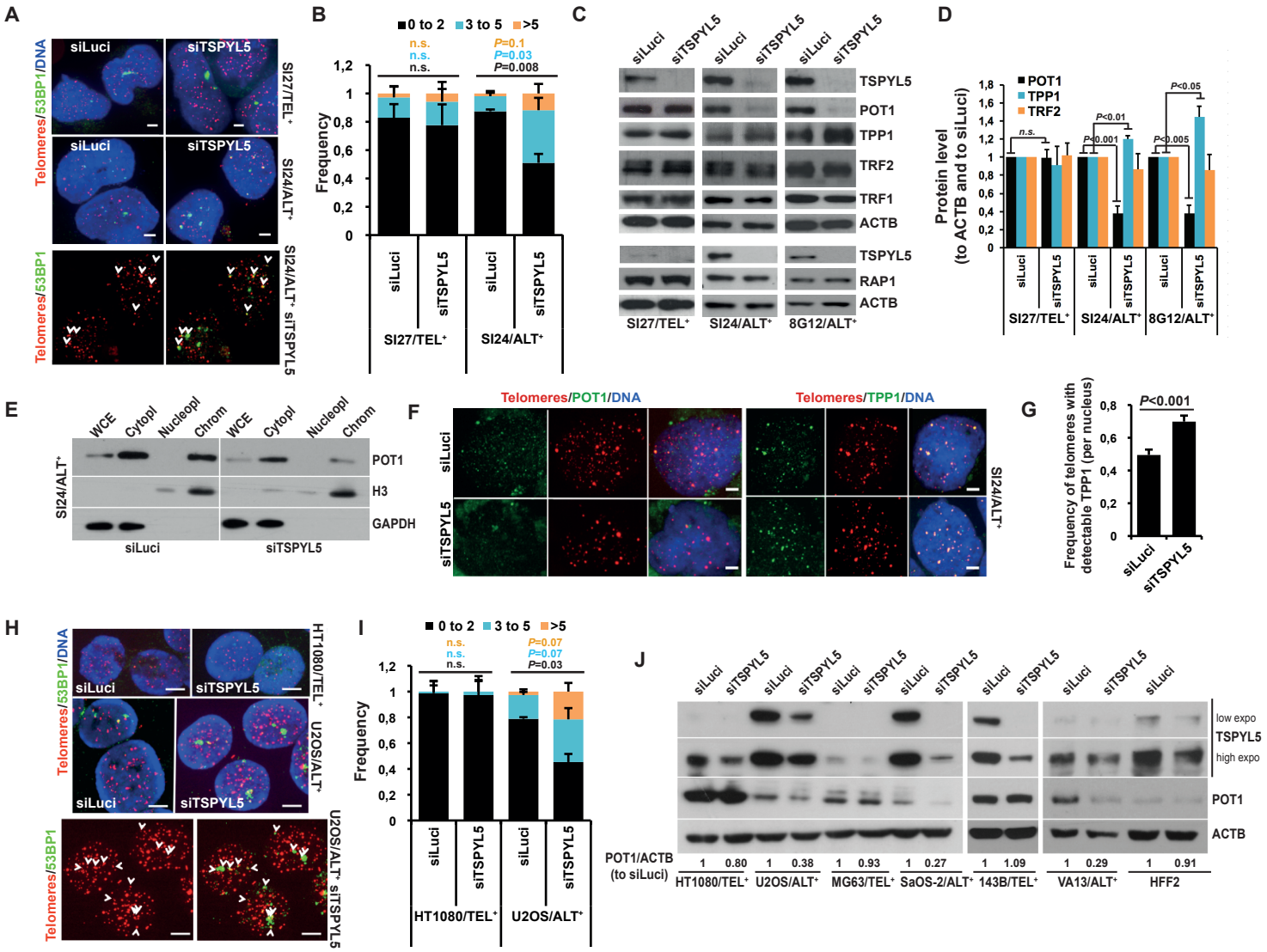

Figure 3

Figure 4

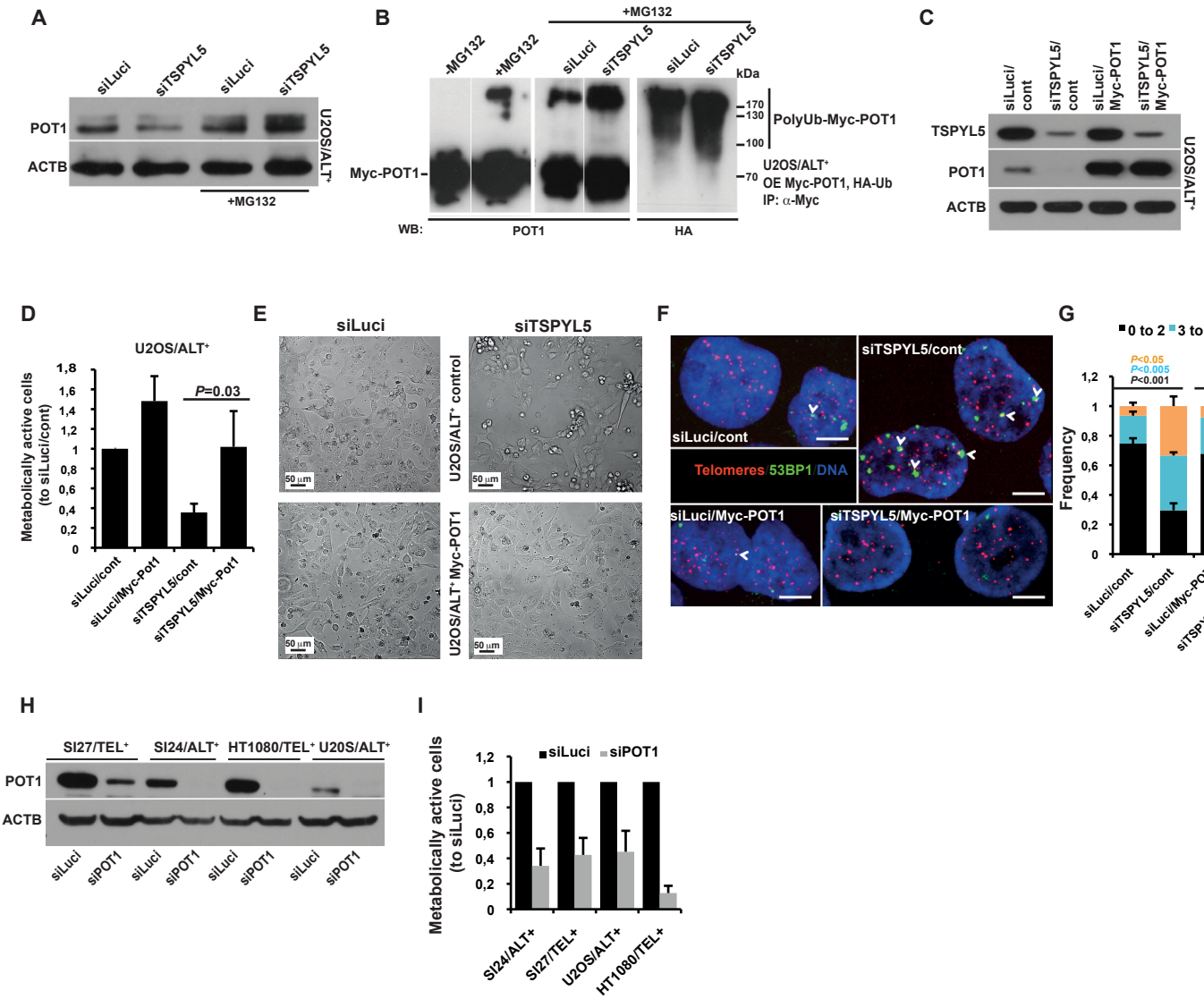

Figure 4

Figure 5

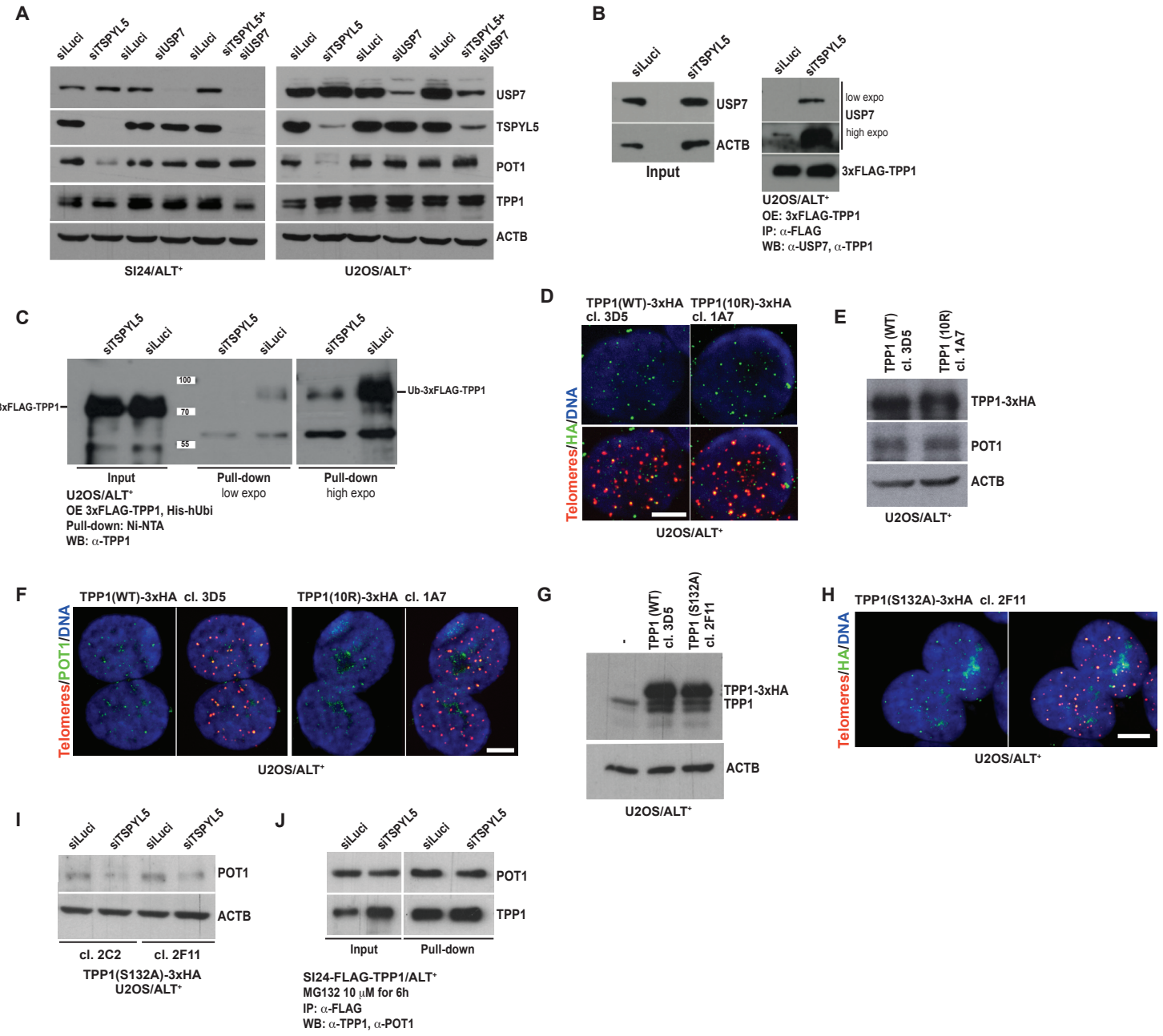

Figure 5

Figure 6

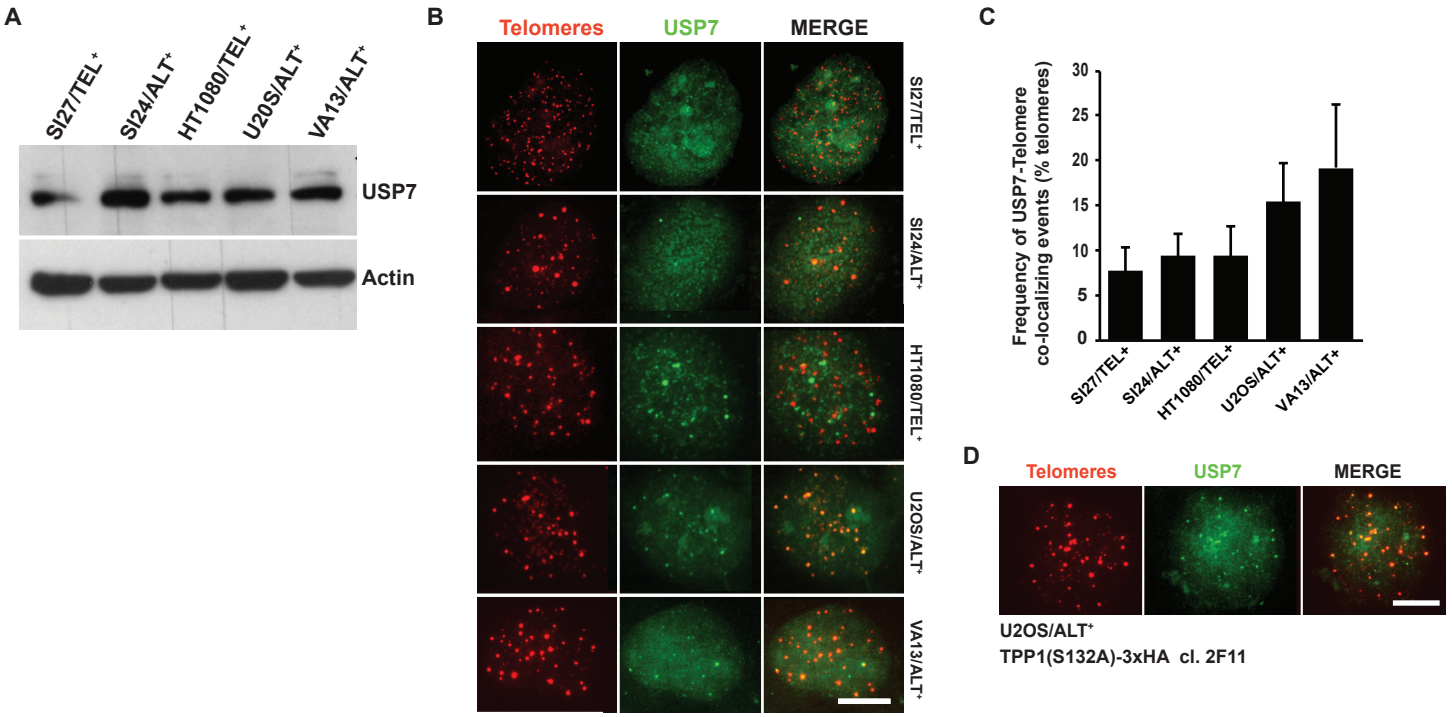

Figure 6

Figure 7

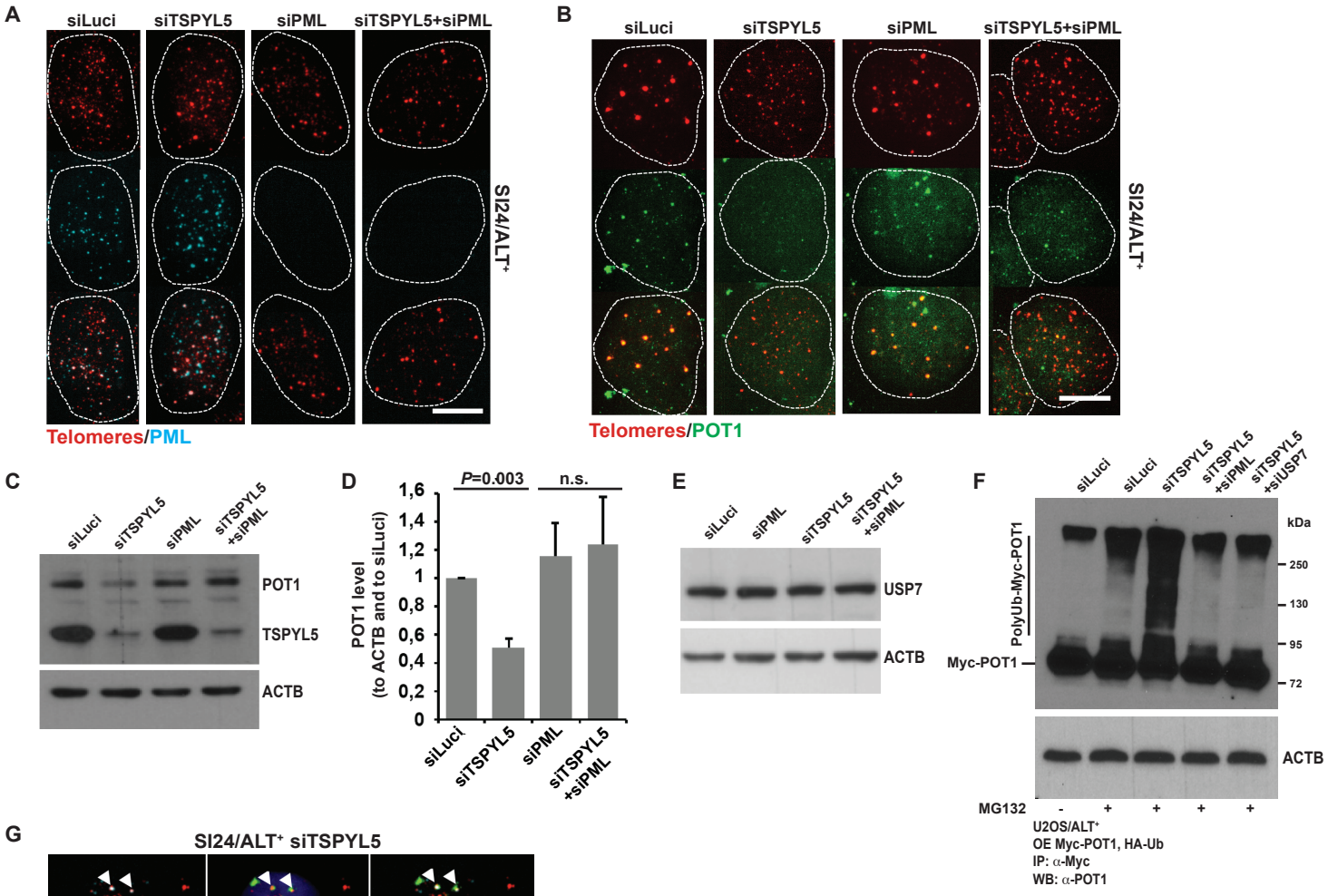

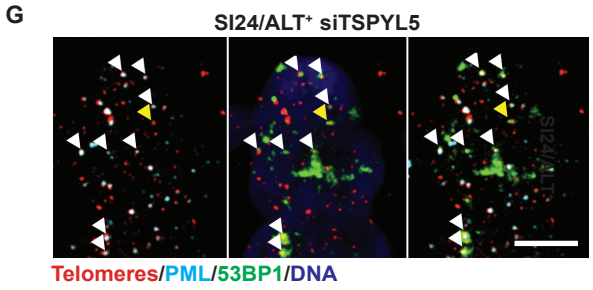

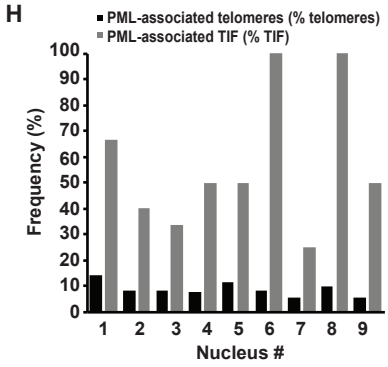

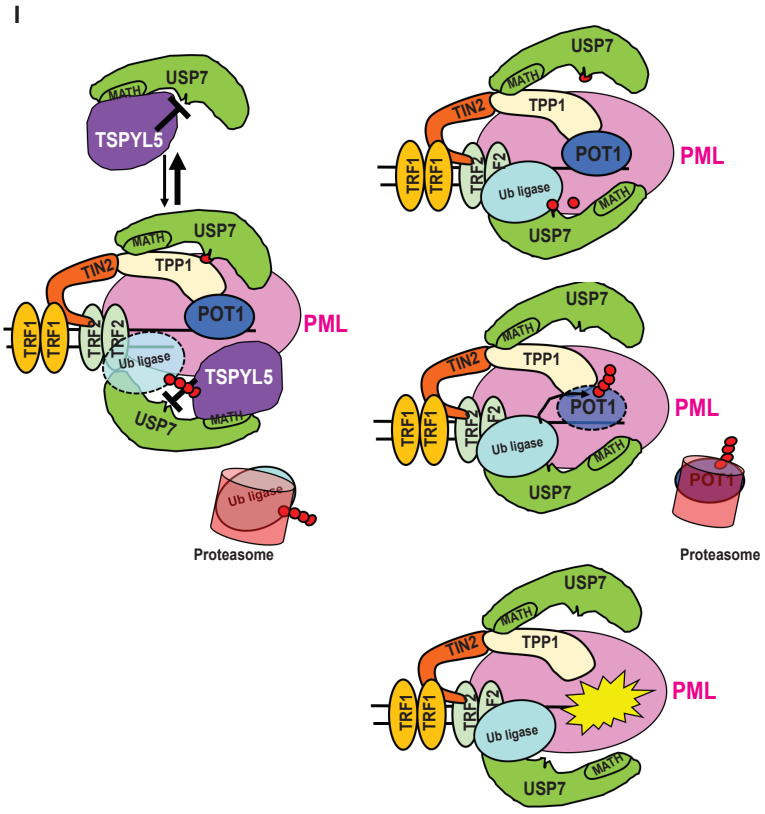

Figure 7

TSPYL5 depletion induces specific death of ALT cells through USP7-dependent proteasomal degradation of POT1

Harikleia Episkopou, Aurélie Diman, Eloïse Claude, Nikenza Viceconte, Anabelle Decottignies

Correspondence to: anabelle.decottignies@uclouvain.be

This file includes:

Figures S1 to S7 with titles and legends
Supplemental Table 1

Figure S1. Related to Figure 1.

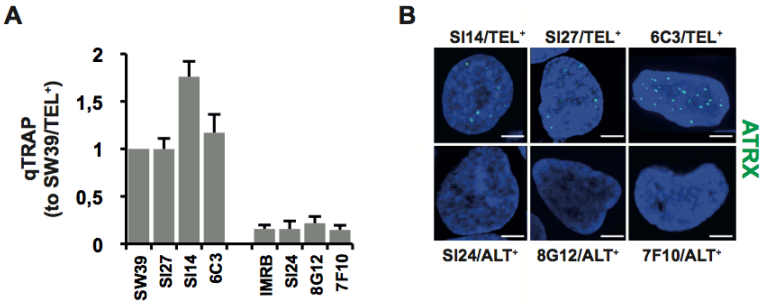

Figure S1. Telomerase activity and ATRX expression in cellular hybrids. (**A**) Telomerase activity measurement by qTRAP. Values were normalized to telomerase activity in SW39/TEL$^+$ cell line. (**B**) Representative images of ATRX staining (green). DNA was stained with DAPI. Bar scale, 10 μm. **Related to Figure 1**

Figure S2. Related to Figure 2.

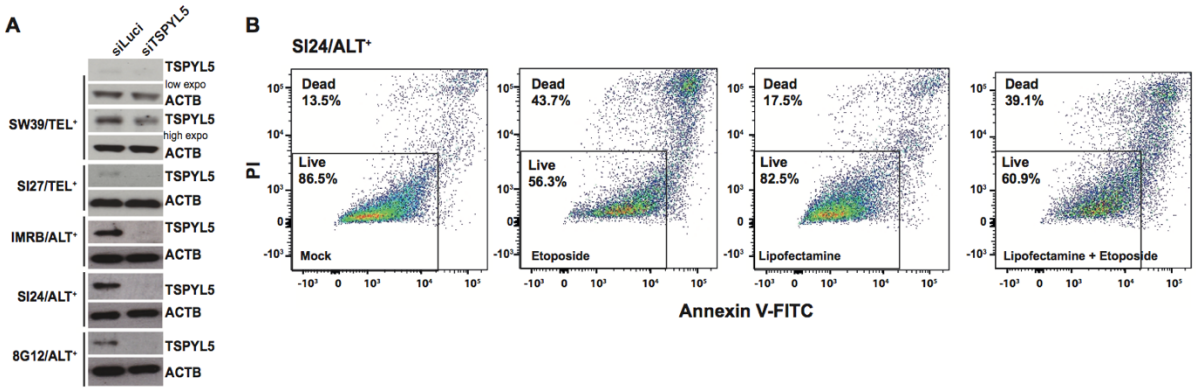

Figure S2. Validation of *TSPYL5* knock-down efficiency and impact of Lipofectamine transfection and etoposide treatment on AnnexinV-FITC staining. (**A**) *TSPYL5* knock-down. Control cells were transfected with siRNA against Luciferase (siLuci). A longer exposure of the membrane is shown for SW39/TEL$^+$ cells with low TSPYL5 expression. (**B**) Representative FACS analyses of Annexin V/FITC staining in SI24/ALT$^+$ cells: untreated (Mock), treated with 50 μM etoposide for 24 hours, mock transfected with Lipofectamine 2000 alone or treated with both Lipofectamine 2000 and etoposide. 10,000 events were recorded. Data indicate that the transfection reagent was responsible for the slight increase in dead cells upon treatment with siLuci observed in Fig. 2B. **Related to Figure 2.**

Figure S3. Related to Figure 2.

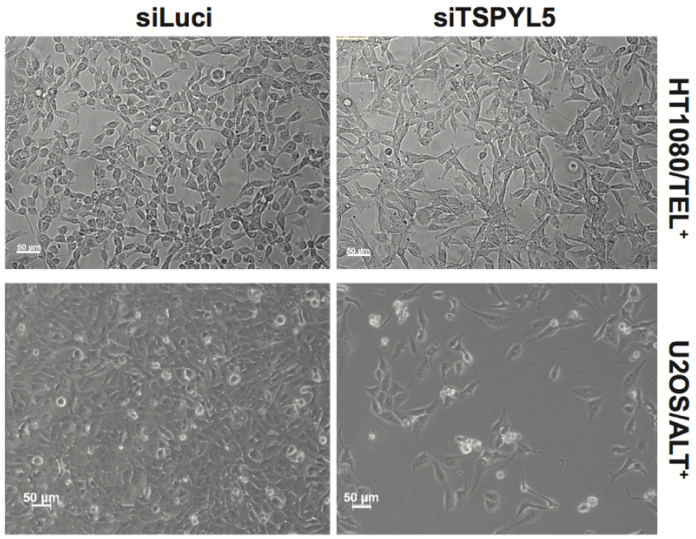

Figure S3. Microscopic observation of cells upon TSPYL5 knock-down. The indicated cell lines were treated with either siLuci or siTSPYL5 for 72 hours before observation with light microscopy. Bar scale, 50 μm. **Related to Figure 2.**

Figure S4. Related to Figure 3.

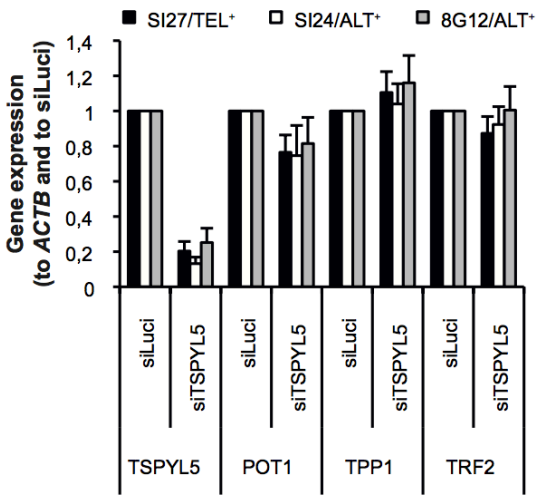

Figure S4. Impact of TSPYL5 knock-down on the expression levels of shelterin genes in SI27/TEL$^+$, SI24/ALT$^+$ and 8G12/ALT$^+$ hybrids. Cell lines were transfected with siTSPYL5 or siLuci (control) for 72 hours before RNA extraction and qRT-PCR against the indicated genes. cDNA levels were normalized first to *ACTB* and then to siLuci-treated samples. Experiments were done in triplicate. **Related to Figure 3.**

Figure S5. Related to Figure 3.

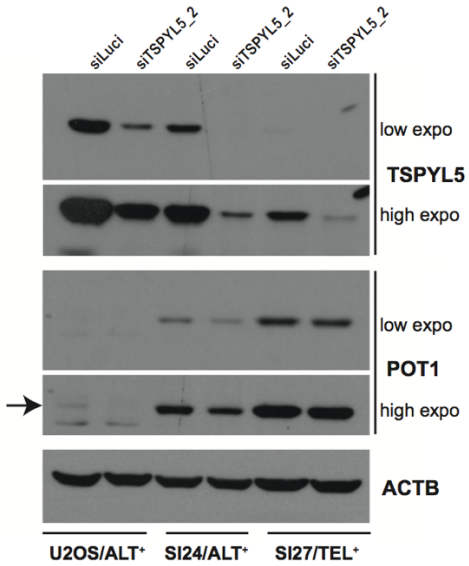

Figure S5. Validation of results using a second siRNA against TSPYL5. Validation of TSPYL5 knock-down with siTSPYL5_2 in U2OS/ALT$^+$, SI24/ALT$^+$ and SI27/TEL$^+$ cells. Control cells were treated with siLuci. Loading control: ACTB. A longer exposure of the membrane is shown to account for cells that express very low levels of TSPYL5. The impact of TSPYL5 knock-down on POT1 levels is shown below. A longer exposure of the membrane is shown to account for the low POT1 levels in U2OS/ALT$^+$ cells. **Related to Figure 3.**

Figure S6. Related to Figure 5.

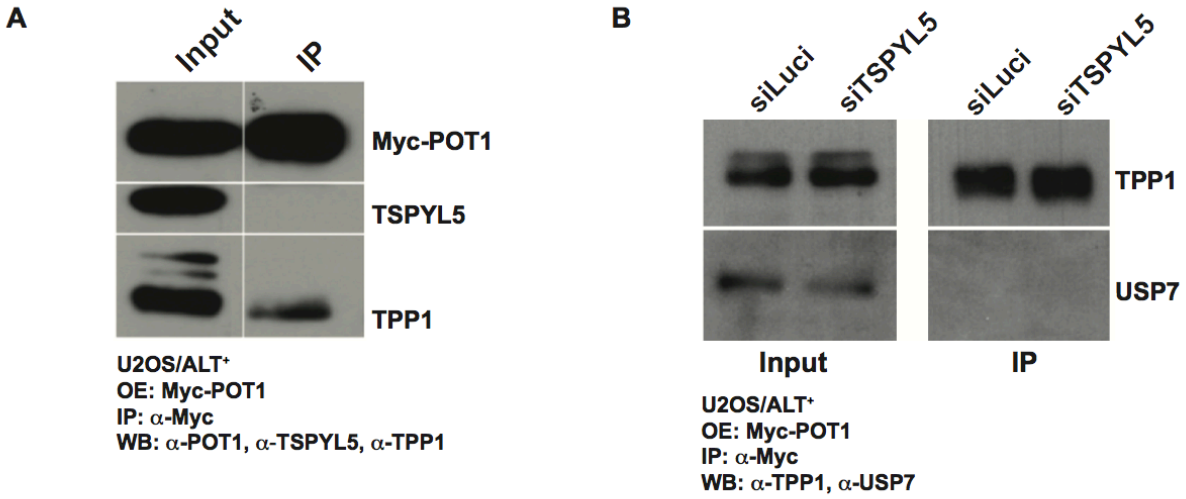

Figure S6. TSPYL5 and USP7 do not directly interact with POT1. (A) Immunoprecipitation using α-Myc antibody in U2OS/ALT$^+$ cells transiently transfected with Myc-POT1 plasmid. WB: α-POT1, α-TSPYL5 and α-TPP1. Input fraction is shown on the left. **(B)** Immunoprecipitation using α-Myc antibody in U2OS/ALT$^+$ cells stably transfected with Myc-POT1 plasmid and treated with the indicated siRNAs for 3 days and with 10 μM MG132 for the last 6 hours. WB: α-TPP1, and α-USP7. Input fraction is shown on the left. **Related to Figure 5.**

Figure S7. Related to Figure 7.

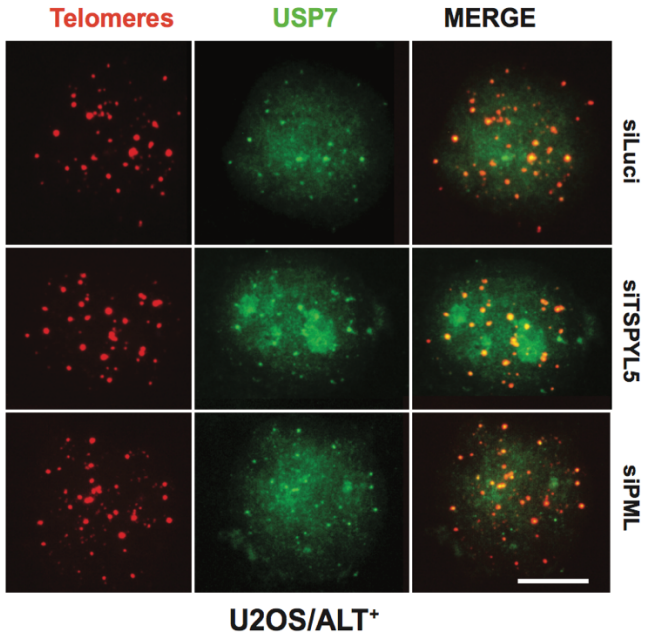

Figure S7. USP7 still localizes to the telomeres of U2OS/ALT$^+$ cells depleted for TSPYL5 or PML. Representative images of telomeres (red FISH probe) and USP7 (green) staining in U2OS/ALT$^+$ cells treated with the indicated siRNAs for 3 days. Bar scale, 10 μm. **Related to Figure 7.**

Supplemental Table 1. Related to Key Resources Table.

Oligonucleotide	Reference
siRNA targeting sequence: TSPYL5 #1: GUACUGAGCUACUUAAACA	Epping *et al*., 2011
siRNA targeting sequence: TSPYL5 #2: GAUAAUCAACGAAGAAUUG	Epping *et al*., 2011
siRNA targeting sequence: USP7: AAUGUGGCCCUGAGUGAUGGA	Li *et al.,* 2004
siRNA targeting sequence: Luciferase: CUUACGCUGAGUACUUCGA	Arnoult *et al*., 2012
ON-TARGETplus Human POT1 siRNA-SMARTpool GUAGAAGCCUUACGUGUUU GAUAAAACAUCGUGGAUUC GCAUAUCCGUGGUUGGAAU UAACUUGCCUGCUCUUUAG	Dharmacon Cat # L-004205-00-0005
siRNA targeting sequence: PML: AGAUGCAGCUGUAUCCAAG	Everett *et al.,* 2006
qRT-PCR primer: TSPYL5 Forward: GCCCAGCTCTGCTTTTACAC	Epping *et al*., 2011
qRT-PCR primer: TSPYL5 Reverse: GCATCTCAAGCTTCTCCTGG	Epping *et al*., 2011
qRT-PCR primer: ACTB Forward: TGTACGCCAACACAGTGCTG	Boros *et al.,* 2014
qRT-PCR primer: ACTB Reverse: GCTGGAAGGTGGACAGCGA	Tilman *et al*., 2009
qRT-PCR primer: POT1 Forward: TCAGTCTGTTAAACTTCATTGCCC	Kondo *et al*., 2004
qRT-PCR primer: POT1 Reverse: TGCACCATCCTGAAAAATTATATCC	Kondo *et al.,* 2004
qRT-PCR primer: TPP1 Forward: CCCGCAGAGTTCTATCTCCA	Poncet *et al.,* 2008
qRT-PCR primer: TPP1 Reverse: GGACAGTGATAGGCCTGCAT	Poncet *et al*., 2008
qRT-PCR primer: TRF2 Forward: GACCTTCCAGCAGAAGATGC	Escoffier *et al*., 2005
qRT-PCR primer: TRF2 Reverse: GTTGGAGGATTCCGTAGCTG	Escoffier *et al.,* 2005
LNA™red probe FISH probe against C-rich telomeric sequences: (TAMRA) GGGTtAGGGttAGgGTTAGGGttAGGGttAGGGtTA(TAMRA) (small letters indicate LNA™ modified bases)	Exiqon
Telomeric probe for TRF: CCCTAACCCTAACCCTAACCCTAA	Viceconte *et al*., 2017
qTRAP assay: primer TS: AATCCGTCGAGCAGAGTT	Viceconte *et al*., 2017
qTRAP assay: primer ACX: GCGCGGCTTACCCTTACCCTTACCCTAACC	Viceconte *et al*., 2017
MSP primer: Methylated TSPYL5 Forward: GAGCGTATATTAGAGAAATTCGTCGA	Jung *et al*., 2008
MSP primer: Methylated TSPYL5 Reverse: GCTATAACCCTACGACTCCTAACG	Jung *et al*., 2008
MSP primer: Unmethylated TSPYL5 Forward: GAGTGTATATTAGAGAAATTTGTTGA	Jung *et al*., 2008
MSP primer: Unmethylated TSPYL5 Reverse: ACTATAACCCTACAACTCCTAACACC	Jung *et al*., 2008